Available online at www.sciencedirect.com
SCIENCE DIRECT®
Journal of Sound and Vibration 262 (2003) 529–562
JOURNAL OF SOUND AND VIBRATION
www.elsevier.com/locate/jsvi

Finite element modelling of piezolaminated smart structures for active vibration control with distributed sensors and actuators

S. Narayanan[a], V. Balamurugan[b,*]

[a] *Department of Applied Mechanics, Indian Institute of Technology Madras, Chennai 600 036, India*
[b] *Centre for Engineering Analysis and Design, Combat Vehicles R&D Establishment, DRDO, Chennai 600 054, India*

Received 18 March 2002; accepted 14 December 2002

Abstract

Finite element modelling of laminated structures with distributed piezoelectric sensor and actuator layers and control electronics is considered in this paper. Beam, plate and shell type elements have been developed incorporating the stiffness, mass and electromechanical coupling effects of the piezoelectric laminates. The effects of temperature on the electrical and mechanical properties and the coupling between them are also taken into consideration in the finite element formulation. The piezoelectric beam element is based on Timoshenko beam theory. The plate/shell element is a nine-noded field-consistent element based on first order shear deformation theory. Constant-gain negative velocity feedback, Lyapunov feedback as well as a linear quadratic regulator (LQR) approach have been used for active vibration control with the structures subjected to impact, harmonic and random excitations. The influence of the pyroelectric effects on the vibration control performance is also investigated. The LQR approach is found to be more effective in vibration control with lesser peak voltages applied in the piezo actuator layers as in this case the control gains are obtained by minimizing a performance index. The application of these elements in high-performance, light-weight structural systems is highlighted.

1. Introduction

The coupled electromechanical properties of piezoelectric ceramics and their availability in the form of thin sheets make them well suited for use as distributed sensors and actuators for controlling structural response. In the sensor application, mechanically or thermally induced

*Corresponding author. Tel.: +91-44-2638-5680; fax: +91-44-2638-3661.
E-mail addresses: narayans@iitm.ac.in (S. Narayanan), balamuruganv@softhome.net (V. Balamurugan).

0022-460X/03/$ - see front matter © 2003 Elsevier Science Ltd. All rights reserved.
doi:10.1016/S0022-460X(03)00110-X

deformations can be determined from measurement of the induced electrical potential (*direct piezoelectric effect*), whereas in actuator applications deformation or strains can be controlled through the introduction of appropriate electric potential (*converse piezoelectric effect*). By integrating distributed piezoelectric sensors/actuators and advanced composites, the potential exists for forming high-strength, high-stiffness, light-weight structures capable of self-monitoring and self-controlling. This technology has numerous applications such as active vibration and buckling control, shape control, damage assessment and active noise control. The developments of these smart structures offer great potential for use in advanced aerospace, hydrospace, nuclear, defence and automotive structural applications. Study of such smart structural systems have been the focus of active research in the recent past.

Distributed vibration control of beams using the piezoelectric effect has been studied by Bailey et al. [1], Crawley and Luis [2] and Tzou [3]. In terms of achieving very high damping, only limited success has been achieved by these distributed control approaches. Tzou has studied the boundary control of beams in Chapter 6 of his recent book [4]. Two control algorithms, namely a displacement feedback and velocity feedback are implemented and their control effectiveness evaluated. It has been shown that velocity feedback controls were much more effective. A one-dimensional mathematical model for determining the mechanical responses of beams with piezoelectric actuators has been proposed by Shen [5]. This model is based on Timoshenko beam theory with the host beam and piezoelectric patches being separately modelled using beam elements. Kinematic assumptions are made to satisfy the compatibility requirements in the vicinity of the interfaces between the piezoelectric devices and the main structure.

The theory of laminated piezoelectric plates for the design of distributed sensors/actuators is given by Lee [6]. He provided governing equations and reciprocal relationships. Structural identification and control of a plate model with distributed piezoelectric sensor/actuator is studied by Tzou and Tseng [7]. They have proposed thin piezoelectric hexahedron finite element with three internal degrees of freedom. Ha et al. [8] have developed an eight-noded three-dimensional composite brick element and studied the response of laminated composites containing distributed piezoelectric ceramics subjected to both mechanical and electrical loadings. Three-dimensional incompatible modes were introduced to take into account the global bending behavior resulting from the local deformations of the piezoceramics. Four-noded, 12-degree-of-freedom plate bending element with one electrical degree of freedom has been proposed by Hwang and Park [9]. In chapter 10 of the book by Tzou [4], a piezoelectric thin hexahedron solid finite element with internal degrees of freedom is presented and applied to distributed sensing and control of continua. A finite element analysis of laminated composite structures containing distributed piezoelectric actuators and sensors has been proposed by Detwiler et al. [10]. The formulation is based on the shear flexible QUAD4 isoparametric element. Static shape control of intelligent structures with distributed piezoelectric sensor/actuator has been proposed by Wang et al. [11]. They have formulated a piezoelectric four-noded plate bending element based on classical plate theory and included the electrical degree of freedom at each node. A finite element model based on classical lamination theory has been developed by Lam et al. [12] for the active vibration control of a composite plate containing distributed piezoelectric sensors/actuators.

Vibration control of composites containing piezoelectric polymers has been studied using finite shell element by Lammering [13]. Classical lamination theory is extended to account for

piezo-electric materials and finite element formulation is based on the shear elastic shell theory of the Reissner–Mindlin type. A generic theory for the intelligent shell system has been developed by Tzou and Gadre [14]. System equations of motion coupling sensing and control effects are derived. Tzou and Ye [15] have analyzed piezoelectric structures with triangular shell elements derived based on the layerwise constant shear angle theory. Saravanos [16] has studied the behavior of composite shell structures. He has developed a shell finite element based on mixed laminate theory that combines single-layer assumption for the displacements and a layerwise representation for the electric potential.

Another area where these piezoelectric materials provide dramatic advantages is in the development of smart structures with the capability to sense thermally induced distortions and to actively compensate for adverse thermomechanical conditions. This coupled thermoelectromechanical behavior of the smart structures with distributed piezoelectric sensors and actuators needs to be understood in order to effectively control such structures. Finite element formulation of thermopiezoelectric beam like structures has been proposed by Rao and Sunar [17] and applied to distributed dynamic measurement and active vibration control. It has been established that thermal effects have an impact on the performance of a distributed control system and the degree of impact may vary depending on the piezoelectric material, the environment where the system operates, and the magnitude of the feedback voltage. Piezothermoelastic effects of distributed piezoelectric sensors/actuator and structural systems are studied by Tzou and Ye [18]. They have investigated distributed controls (static and dynamic) of piezoelectric laminates subjected to a steady state temperature field. Lee and Saravanos [19] have studied the coupled mechanical, electrical and thermal response in modern smart composite beams. The study accounted for thermal effects, which may arise, in the elastic and piezoelectric media at the material level through the constitutive equations. A review of theoretical developments in thermopiezoelasticity having relevance to smart composite structures is presented by Tauchert et al. [20]. The equations governing linear response of piezothermoelastic media are outlined, and a general solution procedure based on potential functions is described.

The present piece of work deals with issues related to finite element modelling of the piezolaminated beam, plate/shell structures including the thermoelectromechanical coupling effects in the constitutive relations. The formulations are based on first order shear deformation theories. The plate/shell element used is derived based on the variationally correct field consistency principle [20] which can be used starting from a thin shell to thick shell, isotropic to laminated composite plate/shells without the need of under-integration of shear and membrane energies. This is one of the unique features of the present work. Also in the present work various control strategies like constant-gain negative velocity feedback and Lyapunov feedback which are classical control theories based on output feedback and a linear quadratic regulator (LQR) scheme which is an optimal control theory based on full state feedback are considered and their relative performance is discussed. This is another unique feature of the present work. This work also considered the pyroelectric effect of the piezoelectric sensors/actuators due to the temperature variation of the environment. The authors' intent is to develop thermopiezoelectric beam, plate/shell finite elements, apply these elements to model beam and plate/shell structures with distributed piezoelectric sensors and actuators and study the active control performance with various control strategies.

2. General layout of the system

A piezoelectric laminated elastic structure as shown in Fig. 1 is considered. Two thin layers of piezoelectric material are bonded on the top and bottom surfaces of the beam. One layer serves as a distributed sensor and the other as a distributed actuator. The effective axis of the piezoelectric layer is aligned with the length and breadth directions of the structure to ensure the maximum piezoelectric effect. The signal from the distributed sensor is used as a feedback reference in a closed-loop feedback control system. The control laws determine the feedback signal to be given to the distributed actuator. In Fig. 1, $F(t)$ is the disturbing force, ϕ_s is the voltage generated by the sensor and ϕ_a is the voltage given to the actuator in order to control the structural deformations. The sensor signal ϕ_s is a function of strains in the structure. The voltage ϕ_a, applied to the actuator, develops effective control forces and moments.

3. Modelling and formulation of the piezolaminated beam element

Fig. 2 shows the piezolaminated beam with distributed PZT sensor and actuator on the top and bottom surfaces. It is assumed that the piezoelectric layers are perfectly bonded to the surface of the beam and also the bonding layers are thin. Hence the contribution of the bonding layers on the mass and stiffness of the beam is negligible. However, the contribution of the piezoelectric sensor and actuator layers on the mass and stiffness of the beam is considered. Timoshenko shear flexible beam theory has been used and perfect continuity without any slip is assumed at the interfaces. The applied voltage is assumed to be uniform along the beam.

3.1. Finite element formulation

The geometry of the beam element indicating the nodal deformations is as shown in Fig. 3. The axial displacement, transverse displacement and transverse rotation of the beam are denoted by u, w and θ_y respectively. x represents the co-ordinate in the axial direction. u, w and θ_y are interpolated using a linear polynomial in x defined over the element length L_e. The local nodal displacements for a typical element (Fig. 3) are given by

$$\{\delta\}_e = \{u_1 \quad w_1 \quad \theta_{y1} \quad u_2 \quad w_2 \quad \theta_{y2}\}^{\mathrm{T}}. \tag{1}$$

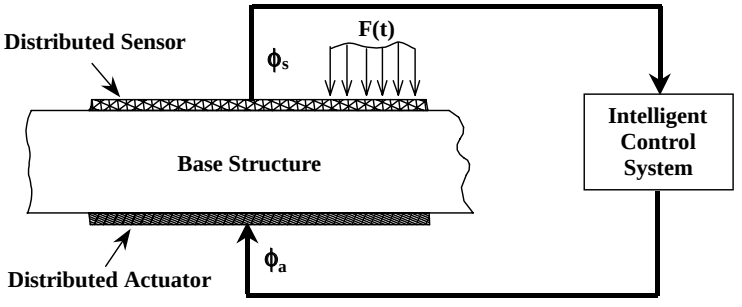

Fig. 1. General layout of the system.

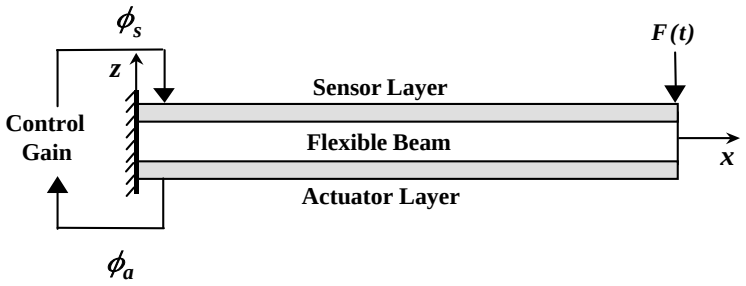

Fig. 2. A cantilever beam with distributed actuator and sensor.

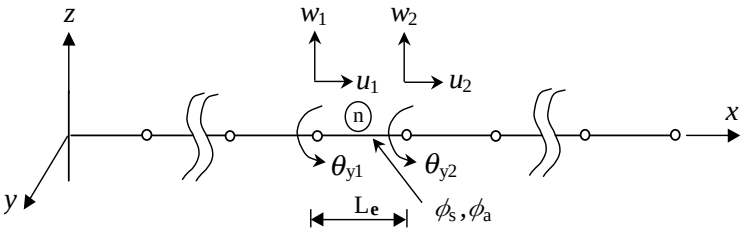

Fig. 3. Finite element discretization of the beam.

The axial displacement, transverse displacement and transverse rotation are expressed in terms of the nodal displacements by finite element shape functions as

$$u = [N_u(x)]\{\delta\}_e, \quad w = [N_w(x)]\{\delta\}_e, \quad \theta_y = [N_{\theta_y}(x)]\{\delta\}_e, \tag{2}$$

where $[N_u(x)], [N_w(x)]$ and $[N_{\theta_y}(x)]$ are the shape functions.

The element stiffness and mass matrices of the beam with the piezoelectric layers are evaluated from the potential and kinetic energies due to the beam deformations and the element force vector due to external disturbance forces is evaluated from the virtual work, in the usual way.

For one-dimensional structures with uniaxial loading, the constitutive equation of the piezoelectric materials coupling elastic and electric fields (IEEE standard on piezoelectricity [21]) can be written as

$$\begin{bmatrix} \epsilon \\ D \end{bmatrix} = \begin{bmatrix} S_{p11} & d_{31} \\ d_{31} & \varepsilon_{33}^{\mathrm{T}} \end{bmatrix} \begin{bmatrix} \sigma \\ \bar{E} \end{bmatrix}, \tag{3}$$

where D is the electrical displacement (charge/area in the beam transverse direction (z direction)), $\bar{E}$ is the electrical field (voltage/length along the transverse direction), ϵ is the mechanical strain in the axial direction (x direction), and σ is the mechanical stress in x direction. S_{p11} is the elastic compliance constant, $\varepsilon_{33}^{\mathrm{T}}$ is the dielectric constant, and d_{31} is the piezoelectric strain constant.

$$S_{p11} = \frac{1}{E_p} \quad \text{and} \quad \bar{E} = \frac{\phi_p(t)}{h_p}, \tag{4}$$

where E_p is the Young's modulus of the piezoelectric material, ϕ_p is the voltage applied (in the case of actuator)/induced (in the case of sensor) in the piezoelectric material and h_p is the thickness of the piezoelectric material (subscript p represents the actuator or sensor piezoelectric layer).

The virtual work done by the induced strain (force) in the actuator is given by

$$\begin{aligned}\Delta W_a &= \int_0^{L_e} E_a d_{31_a} b\phi_a(t)\Delta\left(\frac{\partial u}{\partial x} - r_a\frac{\partial \theta_y}{\partial x}\right)\mathrm{d}x = E_a d_{31_a} b\phi_a(t)(\Delta u - r_a\Delta\theta_y)|_{x=0}^{x=L_e}\\ &= E_a d_{31_a} b\phi_a(t)\{\Delta\delta\}_e^{\mathrm{T}}\left(\begin{bmatrix}[N_u(L_e)]\\ [N_{\theta_y}(L_e)]\end{bmatrix}^{\mathrm{T}}\begin{Bmatrix}1\\ -r_a\end{Bmatrix} - \begin{bmatrix}[N_u(0)]\\ [N_{\theta_y}(0)]\end{bmatrix}^{\mathrm{T}}\begin{Bmatrix}1\\ -r_a\end{Bmatrix}\right)\\ &= \{\Delta\delta\}_e^{\mathrm{T}} E_a d_{31_a} b\phi_a(t)\times\{-1 \quad 0 \quad r_a \quad 1 \quad 0 \quad -r_a\}^{\mathrm{T}} = \{\Delta\delta\}_e^{\mathrm{T}}\{P_a\}_e\phi_a(t),\end{aligned} \tag{5}$$

where $\{P_a\}_e$ is the piezoelectric element force vector which maps the applied actuator voltage to the induced displacements and r_a is the distance measured from the neutral axis of the beam to the mid-plane of the actuator layer (subscript a represents the piezoelectric actuator layer). $\{P_a\}_e$ can be written as

$$\{P_a\}_e = E_a d_{31_a} b\times\{-1 \quad 0 \quad r_a \quad 1 \quad 0 \quad -r_a\}^{\mathrm{T}} = \{-F_a \quad 0 \quad M_a \quad F_a \quad 0 \quad -M_a\}^{\mathrm{T}}. \tag{6}$$

Here, F_a and M_a are the axial control forces and the bending control moments respectively. It can be noted that the piezoelectric induced force and moment results in boundary actions at the ends of the piezoelectric layer due to the force cancellation at common nodes when continuity between elements is enforced.

Using Hamilton's principle, the equations of motion for an element can be obtained as

$$[M]_e\{\ddot{\delta}\}_e + [K]_e\{\delta\}_e = \{f_d\}_e + \{P_a\}_e\{\phi_a(t)\}, \tag{7}$$

where $[M]_e$ is the element mass matrix and $[K]_e$ is the element stiffness matrix obtained from the kinetic and potential energies of the beam with the piezoelectric sensor and actuator layers due to axial and bending deformations. The global equations of motion obtained by assembling the elemental equations is given by

$$[M]\{\ddot{\delta}\} + [C]\{\dot{\delta}\} + [K]\{\delta\} = \{f_d\} + \{P_a\}\{\phi_a(t)\}, \tag{8}$$

where $[C]$ is the structural damping, represented as equivalent viscous damping.

Assuming that the system response is governed by the first m modes of the system, the equations of motion (8) can be transformed, using the modal vector matrix, to the reduced modal space form:

$$[\bar{M}]\{\ddot{\eta}\} + [\bar{C}]\{\dot{\eta}\} + [\bar{K}]\{\eta\} = \{\bar{f}_d\} + \{\bar{P}_a\}\{\phi_a(t)\}, \tag{9}$$

where $[\bar{M}], [\bar{C}]$ and $[\bar{K}]$ are $m\times m$ diagonal matrices because of the orthogonality of the mode shapes with respect to the mass and stiffness matrices. $\{\eta\}$ is the modal displacement vector. In this case $[\bar{C}]$ which is the damping matrix in the modal domain is expressed as

$$\bar{C}_{ij} = 2\xi_i\omega_i \quad \text{for } i = j \quad \text{and} \quad \bar{C}_{ij} = 0 \quad \text{for } i\neq j,$$

where ξ_i is the modal damping factor for the ith mode, and ω_i is the natural frequency for the ith mode. In the numerical calculations, in the present paper, a modal damping factor of 0.2% is assumed for all the modes considered for the response. In order to apply the optimal control

schemes like LQR, it is convenient to have the equations representing the dynamics of the system in a state space form. Introducing the state space variable $\{\xi\}$ as $\{\xi\} = \begin{Bmatrix} \dot{\eta} \\ \eta \end{Bmatrix}$, the system dynamics can be written in state space form as

$$\{\dot{\xi}\} = [A]\{\xi\} + [B]\{\phi_a\} + [\hat{B}]\{u_d\}, \tag{10}$$

where $[A]$ is the system matrix, $[B]$ is the control matrix and $[\hat{B}]$ is the disturbance matrix, which are given by

$$[A] = \begin{bmatrix} -[\bar{M}]^{-1}[\bar{C}] & -[\bar{M}]^{-1}[\bar{K}] \\ [I] & [0] \end{bmatrix}, \quad [B] = \begin{bmatrix} [\bar{M}]^{-1}\{\bar{P}_a\} \\ [0] \end{bmatrix}, \quad [\hat{B}] = \begin{bmatrix} [\bar{M}]^{-1}\{\bar{f}_d\} \\ [0] \end{bmatrix}, \tag{11}$$

$\{u_d\}$ is the disturbance input vector and $\{\phi_a\}$ is the control input (to actuator). The output equation can be written in the physical co-ordinates as $\{y\} = [C_o]\{\delta\}$, where $[C_o]$ is the output matrix. On transforming to modal co-ordinates and then to state space co-ordinates, the output equation could be written as

$$\{\bar{y}\} = [\bar{C}_o]\{\xi\}. \tag{12}$$

The state space model of the system dynamics is thus represented by Eqs. (11) and (12).

3.2. Sensor equations

If the sensor is extending on the beam from $x = x_1$ to $x = x_2$ and $x_2 > x_1$ (Fig. 4) then the sensor voltage ϕ_s contributed by the bending effect can be estimated by the normal strains in the axial direction of the beam. Thus the sensor voltage is given by

$$\phi_s = -\frac{h_s}{x_2 - x_1}\int_{x_1}^{x_2} g_{31} E_s r_s \theta_{y,x}\, \mathrm{d}x = -\frac{h_s}{x_2 - x_1} g_{31} E_s r_s \theta_y|_{x_1}^{x_2}, \tag{13}$$

where h_s is sensor thickness, g_{31} is the piezoelectric stress constant, r_s is the distance measured from the neutral axis of the beam to the mid-plane of the sensor layer and E_s is the Young's modulus of the sensor.

It can be noted from the sensor equation that the output signal is proportional to the rotation of the beam at both ends of the sensor layer. For a fully distributed sensor, that is, $x_1 = 0$ and $x_2 = L$, where L is the length of the beam, the sensor signal becomes

$$\phi_s = -\frac{h_s}{L} g_{31} E_s r_s \theta_y|_0^L. \tag{14}$$

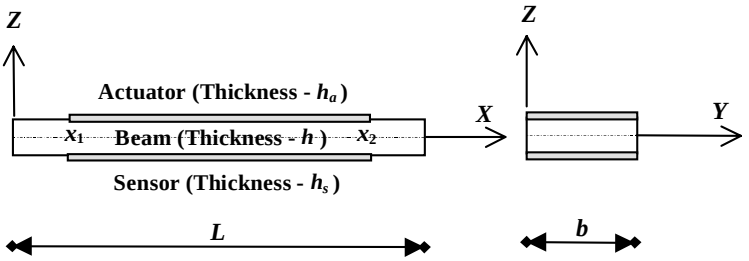

Fig. 4. Layout of the beam with partially covered distributed piezoelectric actuator and sensor.

Note that the sensor signal is zero if the slopes at both ends of the sensor become equal, for example, antisymmetrical modes of a simply supported beam laminated with a symmetrically distributed sensor layer. In such circumstances, segmented sensors and actuators with multi-input–multi-output (MIMO) controllers can be used. After obtaining the sensing signal ϕ_s, the actuator voltage ϕ_a to be applied across the actuator can be determined using any one of the control laws as discussed below.

3.3. Control laws

In the present work two types of classical control laws, which are based on output feedback and one optimal control law based on full state feedback are considered. The classical control laws considered are constant-gain negative velocity feedback and Lyapunov feedback. The optimal control law considered is LQR scheme. In the case of classical control laws the gains are arbitrarily chosen, whereas in the case of optimal control law, an optimal control gain is obtained, which minimizes an objective function. Brief descriptions of the control laws are as given below.

3.3.1. Constant-gain negative velocity feedback

In this method of control, the sensor signal ϕ_s is differentiated so that a strain rate (related to the velocity) information is obtained and the actuator voltage ϕ_a is given by

$$\phi_a(t) = -G_c\dot{\phi}_s(t). \tag{15}$$

The velocity feedback can enhance the system damping and therefore effectively control the oscillation amplitude. But as the velocity amplitude decays the feedback voltage also decreases. This will reduce the effectiveness at low vibration levels for a given voltage limit.

3.3.2. Lyapunov feedback

In Lyapunov feedback control, the feedback voltage amplitude is constant but the sign is opposite to the velocity. The amplitude of feedback signal can be expressed as

$$\phi_a(t) = -\phi_{max}\,\mathrm{sgn}[\dot{\phi}_s(t)], \tag{16}$$

where sgn[.] is a signum function and ϕ_{max} is the magnitude of the control voltage. This is also called bang–bang control. Note that the Lyapunov control scheme can introduce unstable oscillations due to sudden change of feedback voltage and hence a dead zone is set up, as in the equation below to prevent excessive chattering:

$$\phi_a(t) = 0 \quad \text{when} \quad -\phi_{dead} < \phi_s < \phi_{dead}. \tag{17}$$

3.3.3. LQR optimal control

Linear quadratic regulator (LQR) optimal control theory [22,23] is used to determine the control gains. In this, the feedback control system is designed to minimize a cost function or a performance index which is proportional to the required measure of the system's response. A state feedback rather than output feedback is adopted to enhance the control performance. The cost function used in this case is given by

$$J = \int_0^\infty (\{\bar{y}\}^{\mathrm{T}}[Q]\{\bar{y}\} + \{\phi_a\}^{\mathrm{T}}[R]\{\phi_a\})\,\mathrm{d}t, \tag{18}$$

where $[Q]$ and $[R]$ are the semi-positive-definite and positive-definite weighting matrices on the outputs and control inputs, respectively. Larger (relatively) elements in $[Q]$ mean that we demand more vibration suppression ability from the controller. The purpose of the second term in Eq. (18) is to account for the *effort* being expended by the control system, so that small reductions in the output response are not obtained at the expense of physically unreasonable actuator input levels. Assuming full state feedback, the control law is given by

$$\{\phi_a\} = -[G_c]\{\xi\} = -[R]^{-1}[B]^{\mathrm{T}}[\hat{P}]\{\xi\}, \tag{19}$$

where $[G_c]$ is the control gain.

$[\hat{P}]$ can be obtained by the solution of the Riccati equation given by

$$[A]^{\mathrm{T}}[\hat{P}] + [\hat{P}][A] - [\hat{P}][B][R]^{-1}[B]^{\mathrm{T}}[\hat{P}] + [C_o]^{\mathrm{T}}[Q][C_o] = 0. \tag{20}$$

The closed-loop system dynamics is given by

$$\{\dot{\xi}\} = ([A] - [B][G_c])\{\xi\} + [\hat{B}]\{u_d\} = [A_{cl}]\{\xi\} + [\hat{B}]\{u_d\}, \tag{21}$$

where $[A_{cl}]$ is the closed-loop system matrix. The eigen values of $[A_{cl}]$ gives the damped natural frequencies and damping ratios.

It can be noted that only few states of the system can be measured as the output of the sensor, while all states of the system are used in obtaining the actuator voltage. Hence a *state observer* or *estimator* is to be designed which can estimate all the state values from the measured signal. One such observer is the *Kalman filter* which is an optimal state observer for a system contaminated with process and measurement noise. An optimal control procedure that uses a Kalman filter as an observer and a controller that minimizes a cost function of quadratic form is called an LQG control method [22,23]. The *MATLAB* software has inbuilt functions for estimating the control gains using LQR and LQG methods. In the present work, *MATLAB* software has been used for solving the associated Riccati equation and obtaining the control gains in the cases of LQR control methods.

3.4. Actuator equations

For a distributed piezoelectric actuator, as discussed in Eqs. (5) and (6), the distributed control force F_a and control moment M_a acting on the beam are given by

$$F_a = E_a d_{31_a} b\phi_a, \quad M_a = r_a E_a d_{31_a} b\phi_a. \tag{22}$$

It can be noted that the control forces and moments are spatially distributed when the actuator thickness is not uniform throughout. In the case when the control moments are not spatial functions, the control effects can be introduced from boundaries via the boundary control. That is, in the case of a cantilever beam the control moment can be assumed to be applied at the free end whose magnitude is given by M_a.

4. Modelling and formulation of the piezolaminated plate/shell element

A composite shell structure is considered with thin PZT piezoceramic layers embedded on top and bottom surfaces. A °C continuous, shear flexible, nine-noded quadrilateral shell element

derived based on field consistency principle [24] has been used and has been developed to include the stiffness, mass and thermoelectromechanical coupling effects of the piezoelectric sensor and actuator layers.

4.1. Constitutive relations

The linear constitutive equations coupling elastic field, electric field and thermal field in piezoelectric medium is expressed by the direct and converse piezoelectric equations [17]. These equations for the plate shape sensor and actuator are written as

$$\{\sigma\} = [C]\{\epsilon\} - [e]^{\mathrm{T}}\{E\} - \{\lambda\}\Theta, \quad \{D\} = [e]\{\epsilon\} + [\varepsilon]\{E\} + \{P\}\Theta, \tag{23}$$

where $\{D\}$, $\{E\}$, $\{\lambda\}$, $\{P\}$, $\{\epsilon\}$ and $\{\sigma\}$ are electrical displacement, electrical field, stress coefficient of thermal expansion, pyroelectric coefficients, strain and stress vectors respectively. $[C]$, $[e]$ and $[\varepsilon]$, are elasticity, piezoelectric and dielectric constant matrices respectively. Θ is the global temperature variation in °C.

4.2. Finite element formulation

A doubly curved shell is considered (Fig. 5) [25] with co-ordinates x, y along the inplane direction and z along the thickness direction. Using the Mindlin formulation, the displacement u, v and w at a point (x, y, z) from the median surface are expressed as function of mid-plane displacements u_o, v_o, w and independent rotations θ_x and θ_y of normal in xz and yz planes, respectively, as

$$\begin{aligned} u(x, y, z, t) &= u^o(x, y, t) + z\theta_x(x, y, t), \\ v(x, y, z, t) &= v^o(x, y, t) + z\theta_y(x, y, t), \\ w(x, y, z, t) &= w(x, y, t). \end{aligned} \tag{24}$$

Assuming small deformation and considering the effect of shear deformation, the total strain could be expressed as

$$\{\epsilon\} = \begin{Bmatrix} \epsilon_p \\ 0 \end{Bmatrix} + \begin{Bmatrix} z\epsilon_b \\ \epsilon_s \end{Bmatrix}, \tag{25}$$

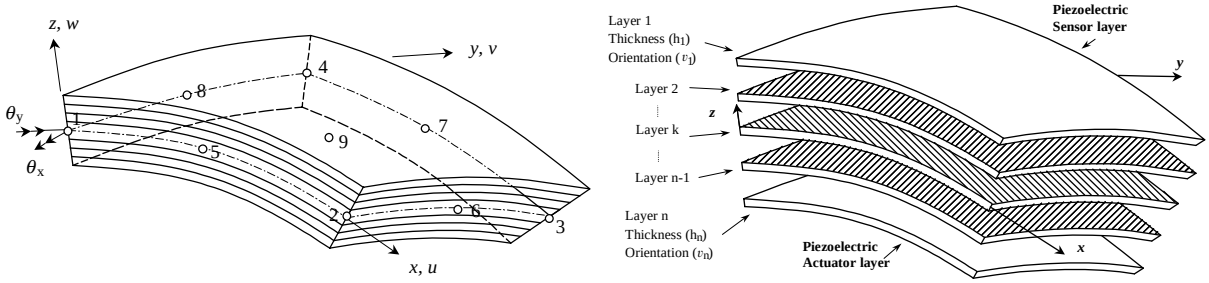

Fig. 5. Doubly curved piezolaminated nine-noded composite shell element.

where $\{\epsilon_p\}$ are the mid-plane (membrane) strains, $\{\epsilon_b\}$ are the bending strains and $\{\epsilon_s\}$ are the shear strains [25] and are written as

$$\{\epsilon_p\} = \begin{Bmatrix} u^o_{,x} + (w/R_x) \\ v^o_{,y} + (w/R_y) \\ u^o_{,y} + v^o_{,x} + (2w/R_{xy}) \end{Bmatrix}, \quad \{\epsilon_b\} = \begin{Bmatrix} \theta_{x,x} \\ \theta_{y,y} \\ \theta_{x,y} + \theta_{y,x} - u^o_{,y}/R_x - v^o_{,x}/R_y \end{Bmatrix},$$
$$\{\epsilon_s\} = \begin{Bmatrix} \theta_x - w_{,x} + u^o/R_x + v^o/R_{xy} \\ \theta_y - w_{,y} + v^o/R_y + u^o/R_{xy} \end{Bmatrix}. \tag{26}$$

In general, the electrical field $\{E\}$ is expressed as $\{E\} = \{E_x \quad E_y \quad E_z\}^{\mathrm{T}} = -\{\phi_{,x} \quad \phi_{,y} \quad \phi_{,z}\}^{\mathrm{T}}$. This element has five elastic degrees of freedom u^o, v^o, w, θ_x, θ_y per node, one temperature degree of freedom, θ per node and one electrical degree of freedom, ϕ per piezoelectric layer, that is, the electric potential ϕ is assumed to be constant over an element and varying linearly through the thickness of the piezoelectric layer.

The electric field strength considering a piezoelectric sensor and actuator layers is given by

$$\{-E\} = [B_\phi]\{\phi\} = \begin{bmatrix} 0 & 0 & (1/t_s) & 0 & 0 & 0 \\ 0 & 0 & 0 & 0 & 0 & (1/t_a) \end{bmatrix}^{\mathrm{T}} \begin{Bmatrix} \phi_s \\ \phi_a \end{Bmatrix}, \tag{27}$$

where t_s and t_a are the thicknesses of the piezoelectric sensor and actuator layers respectively. Using standard discretization techniques in an element the displacement field can be expressed in terms of shape functions [26]. The thermal field is also expressed in terms of a similar set of shape functions as used for the elastic displacements. The piezoelectric sensor and actuator layers are considered as additional laminae of a composite laminate.

For a piezolaminated composite laminate, if $\{F\}$ represents the membrane stress resultants (F_{xx}, F_{yy}, F_{xy}), and $\{M\}$ represents the bending stress resultants (M_{xx}, M_{yy}, M_{xy}), we can relate these to membrane strains, $\{\epsilon_p\}$, and bending strain strains (curvature), $\{\epsilon_b\}$, through the constitutive relation as

$$\{F\} = [A_{ij}]\{\epsilon_p\} + [B_{ij}]\{\epsilon_b\} - \int_{t_p} [e]^{\mathrm{T}}\{E\}\,\mathrm{d}z - \int_{t_p} \{\lambda\}\Theta\,\mathrm{d}z,$$
$$\{M\} = [B_{ij}]\{\epsilon_p\} + [D_{ij}]\{\epsilon_b\} - \int_{t_p} z[e]^{\mathrm{T}}\{E\}\,\mathrm{d}z - \int_{t_p} z\{\lambda\}\Theta\,\mathrm{d}z, \tag{28}$$

where t_p is the thickness of the piezoelectric layer, $[A_{ij}]$, $[B_{ij}]$ and $[D_{ij}]$ $(i,j = 1, 2, 6)$ are extensional, bending-extensional and bending stiffness coefficients of the composite laminate [27]. It is assumed that shear stress is not influencing the piezoelectric effect. If $\{S_{ij}\}$ represents the transverse shear force resultant (S_{xz}, S_{yz}), then it is related to the transverse shear strain through the constitutive relation

$$\{S\} = [E_{ij}]\{\epsilon_s\}, \tag{29}$$

where $[E_{ij}]$ $(i,j=4,5)$ are transverse shear stiffness coefficients of the laminate [27]. Using the variational principles the strain energy functional, U is given by

$$U = \frac{1}{2}\int_A [\{\epsilon_p\}^T[A_{ij}]\{\epsilon_p\} + \{\epsilon_p\}^T[B_{ij}]\{\epsilon_b\} + \{\epsilon_b\}^T[B_{ij}]\{\epsilon_p\} + \{\epsilon_b\}^T[D_{ij}]\{\epsilon_b\} + \{\epsilon_s\}^T[E_{ij}]\{\epsilon_s\}]\,\mathrm{dA} - \int_{V_p}(\{\epsilon_p\}^T + z\{\epsilon_b\}^T)[e]^T\{E\}\,\mathrm{d}V - \int_{V_p}(\{\epsilon_p\}^T + z\{\epsilon_b\}^T)\{\lambda\}\Theta\,\mathrm{d}V. \tag{30}$$

The element electrical energy is given by

$$W^e = \frac{1}{2}\int_{V_p}\{E\}^T\{D\}\,\mathrm{d}V = \frac{1}{2}\int_{V_p}\{E\}^T\{[e]\{\epsilon\} + [\varepsilon]\{E\} + \{P\}\Theta\}\,\mathrm{d}V, \tag{31}$$

where V_p is the volume of the piezoelectric layer in an element.

The virtual work done by the surface force and the applied electrical charge is given by

$$\Delta W^s = \int_{S1}\{\Delta\bar{u}\}^T\{f_s\}\,\mathrm{d}s - \int_{S2}\{\Delta E\}^T\{q\}\,\mathrm{d}s, \tag{32}$$

where $\{f_s\}$ and $\{q\}$ are the surface force intensity and surface electrical charge density respectively. $S1$ and $S2$ are the surface areas where the surface forces and electrical charge are applied respectively.

The element kinetic energy is given by

$$T = \frac{1}{2}\int_A [P(\dot{u}^{o2} + \dot{v}^{o2} + \dot{w}^{o2}) + I(\dot{\theta}_x^2 + \dot{\theta}_y^2)]\,\mathrm{d}A, \tag{33}$$

where A is the area of the element and

$$P = \sum_{k=1}^{n}\int_{-h_{k-1}}^{h_k}\rho\,\mathrm{d}z, \quad I = \sum_{k=1}^{n}\int_{-h_{k-1}}^{h_k} z^2\rho\,\mathrm{d}z; \tag{34}$$

n is the number of layers.

It is assumed that the dynamic coupling of heat transfer with structural deflection and electric field are small. The temperature field can be calculated based on the given thermal excitation using the principles of heat transfer. In the present study, the temperature field is assumed to be known and steady. With these assumptions, using Hamilton's principle, Langrange's equations of motion, for an element can be written as

$$[M_{uu}]_e\{\ddot{\delta}\}_e + [K_{uu}]_e\{\delta\}_e + [K_{u\phi}]_e\{\phi\}_e - [K_{u\theta}]_e\{\theta\}_e = \{F_s\}_e, \tag{35}$$

$$[K_{\phi u}]_e\{\delta\}_e + [K_{\phi\phi}]_e\{\phi\}_e + [K_{\phi\theta}]_e\{\theta\}_e = \{F_q\}_e, \tag{36}$$

where $[M_{uu}]_e$ is the element mass matrix and $[K_{uu}]_e$ is the element elastic stiffness matrix obtained from the kinetic energy and strain energy functional [26]. $[K_{\phi u}]_e = [K_{u\phi}]_e^T$ are the elastic–electric coupling stiffness matrices and $[K_{\phi\phi}]_e$ is the electric stiffness matrix, $[K_{u\theta}]_e$ is the elastothermal stiffness matrix and $[K_{\phi\theta}]_e$ is the electrothermal stiffness matrix. $\{F_s\}_e$ is the applied mechanical

force and $\{F_q\}_e$ is the applied electrical charge. From Eqs. (35) and (36) we get

$$[M_{uu}]_e\{\ddot{\delta}\}_e + [[K_{uu}]_e - [K_{u\phi}]_e[K_{\phi\phi}]_e^{-1}[K_{\phi u}]_e]\{\delta\}_e = \{F_s\}_e + [[K_{u\theta}]_e - [K_{u\phi}]_e[K_{\phi\phi}]_e^{-1}[K_{\phi\theta}]_e]\{\theta\}_e - [K_{u\phi}]_e[K_{\phi\phi}]_e^{-1}\{F_q\}_e. \quad (37)$$

When Eq. (36) is applied to sensors, where the external applied charge is zero, the sensed voltage is given by

$$\{\phi_s\}_e = -[K_{\phi\phi}]_{se}^{-1}([K_{\phi u}]_{se}\{\delta_s\}_e + [K_{\phi\theta}]_{se}\{\theta\}_e), \quad (38)$$

where subscript 's' denotes the sensor layer. The global equations of motion can be obtained by assembling the elemental equations and is given by

$$[M_{uu}]_e\{\ddot{\delta}\} + [C_{uu}]_e\{\dot{\delta}\} + [[K_{uu}] - [K_{u\phi}][K_{\phi\phi}]^{-1}[K_{\phi u}]]\{\delta\} = \{F_s\} + \{F_{eth}\} + \{F_{pth}\} - [K_{u\phi}]\{\phi_a\}, \quad (39)$$

where $\{F_{eth}\}$ and $\{F_{pth}\}$ are the thermal force vectors due to the thermal strain effect and pyroelectric effect, respectively, which are given by

$$\{F_{eth}\} = [K_{u\theta}]\{\theta\}, \quad \{F_{pth}\} = -[K_{u\phi}][K_{\phi\phi}]^{-1}[K_{\phi\theta}]\{\theta\}. \quad (40)$$

Here, $[M_{uu}], [K_{uu}], ([K_{u\phi}] = [K_{\phi u}]^{\mathrm{T}}), [K_{\phi\phi}], [K_{u\theta}], [K_{\phi\theta}]$ and $\{F_s\}$ are the corresponding global quantities, $\{\phi_a\}$ is the actuator voltage vector and $[C_{uu}]$ is the internal structural damping.

Using normal mode transformation and introducing state space variables, the equations of motion can be written as

$$\{\dot{\xi}\} = [A]\{\xi\} + [B]\{\phi_a\} + [\hat{B}]\{u_d\} + [B^{th}], \quad \{\bar{y}\} = [\bar{C}_o]\{\xi\}, \quad (41)$$

where $[A]$ is the system matrix, $[B]$ is the control matrix $[\hat{B}]$ is the disturbance matrix and $[B^{th}]$ is the thermal disturbance matrix which are given by

$$[A] = \begin{bmatrix} -[\bar{M}]^{-1}[\bar{C}] & -[\bar{M}]^{-1}[\bar{K}] \\ [I] & [0] \end{bmatrix}, \quad [B] = \begin{bmatrix} -[\bar{M}]^{-1}[\bar{K}_{u\phi}] \\ [0] \end{bmatrix},$$
$$[B] = \begin{bmatrix} [\bar{M}]^{-1}\{\bar{F}_s\} \\ [0] \end{bmatrix}, \quad [B^{th}] = \begin{bmatrix} [\bar{M}]^{-1}\{\{\bar{F}_{eth}\} + \{\bar{F}_{pth}\}\} \\ [0] \end{bmatrix}, \quad (42)$$

$\{u_d\}$ is the disturbance input vector and $\{\phi_a\}$ is the control input and $\{y\}$ is the output vector.

LQR optimal control theory [22] as detailed in Section 3.3, is used to determine the active control gains.

5. Results and discussion

5.1. Vibration control using piezolaminated beam elements

The piezolaminated beam element has been validated for sensing and actuation performance [28]. After validating the present formulation, the vibration control study has been made using a steel cantilever beam (Fig. 6) of dimension 0.5 m × 0.03 m × 0.002 m. Two PZT layers of thickness 40 μm are bonded on top and bottom surfaces of the beam to act as a sensor and actuator

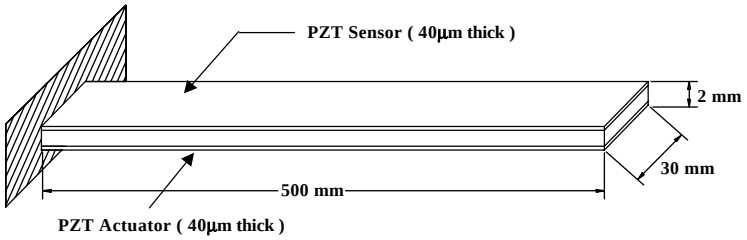

Fig. 6. A steel cantilever beam with distributed PZT sensor and actuator.

Table 1
Material properties of the piezoelectric materials used

Property name	PVDF	PZT
Young's modulus (N/m^2)	2×10^9	139×10^9
Density (kg/m^3)	1800	7500
Strain constant (d_{31}) (m/V)	23×10^{-12}	11×10^{-11}
Stress constant (g_{31}) (V m/N)	0.216	0.010
Maximum electric field (V/μm)	30	1

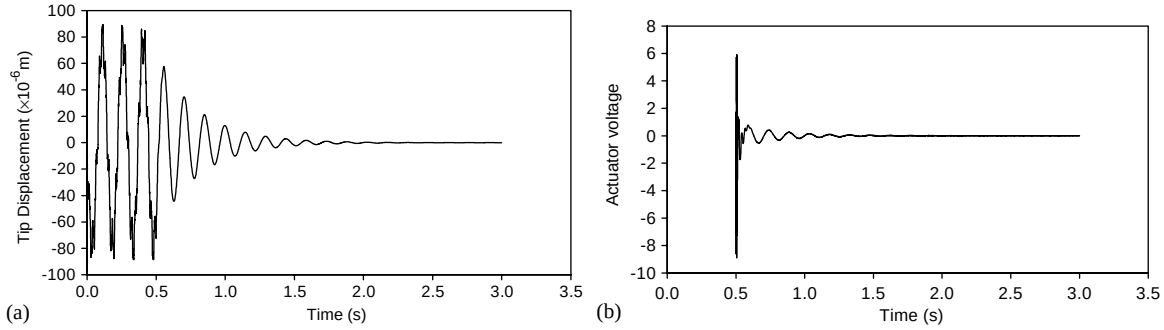

Fig. 7. (a) Tip displacement of piezolaminated cantilever beam subjected to 0.2 N impact load at the tip and controlled using constant-gain negative velocity feedback (gain = 1). (b) The actuator voltage.

respectively. The properties of PZT [29] are given in the Table 1. The beam is divided into 10 elements. The stiffness and the mass of the piezoelectric layers are included in the model. The structural damping is neglected in this case, as the aim is to access the effectiveness of the active control. The first six natural frequencies of the beam are 6.89, 43.285, 121.225, 237.72, 393.58 and 589.63 Hz.

An external impulse load of 0.2 N is assumed to act at the free end of the beam for 1 ms duration. The control is applied after 0.5 s of the application of the load, so as to have a comparison between the controlled and uncontrolled response. The control performance with constant-gain negative velocity feedback with gain 1 and 2 are shown in Figs. 7 and 8 respectively. Fig. 9 indicates the damping ratios versus the gain for the constant-gain negative velocity feedback. It can be noted that the damping ratio increases and reaches a maximum value and then

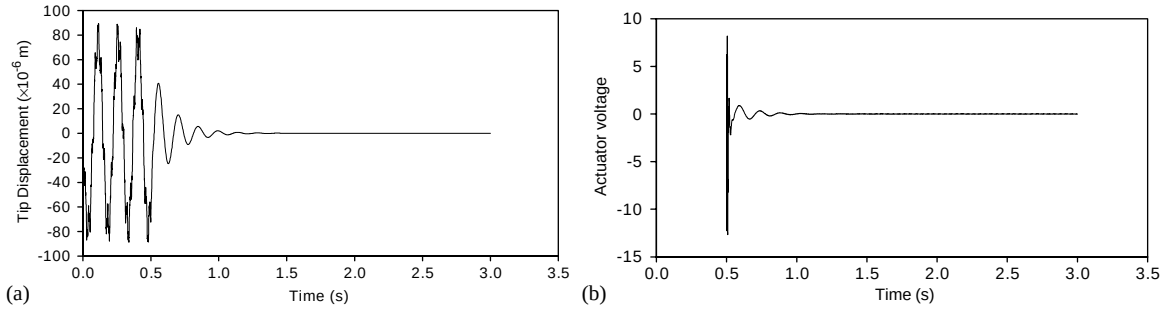

Fig. 8. (a) Tip displacement of piezolaminated cantilever beam subjected to 0.2 N impact load at the tip and controlled using constant-gain negative velocity feedback (gain = 2). (b) The actuator voltage.

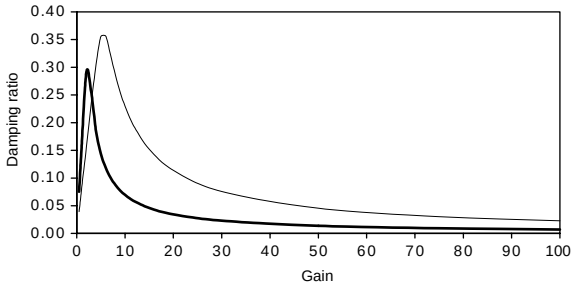

Fig. 9. The damping ratio versus gain of the constant-gain negative velocity feedback control (—— first mode; —— second mode).

decreases with the increase of the gain. This is due to high boundary feedback control effects at the free end. As explained earlier, the distributed piezoelectric actuator applies a counteracting moment to the cantilever beam at the free end when a feedback voltage is applied to the actuator. As the feedback voltage becomes higher and higher the free end is further constrained and the boundary condition gradually changes to a sliding-roller boundary condition [4]. Another point to be kept in mind is that the actuator voltage should not exceed the breakdown voltage of the actuator (at which it will loose its piezoelectric property).

Figs. 10–12 illustrate the control effectiveness due to Lyapunov feedback with a feedback voltage of 0.1, 1 and 9 V respectively. It can be noted that Lyapunov feedback is more effective in controlling the vibration when compared to the constant-gain negative velocity feedback when sufficient feedback voltage is applied. But the energy input is greater than that of the former case. The inherent drawback of the Lyapunov feedback which is also called a bang–bang control is that regardless of how small the feedback gain is, we expect to see a small amount of the residual oscillations. Fig. 12 indicates that the vibration levels are reduced faster but low-amplitude residual oscillation persists. This is due to a high feedback voltage being applied to the actuator which also takes the direction opposite to the instantaneous direction of the velocity.

Figs. 13–15 indicate the control effectiveness using LQR optimal control with weighting factor Q to be 10^8, 10^9 and 10^{10} respectively. The first mode damping factors in these cases respectively are 0.0589, 0.1742 and 0.3815. The damping ratios and the peak actuator voltages for

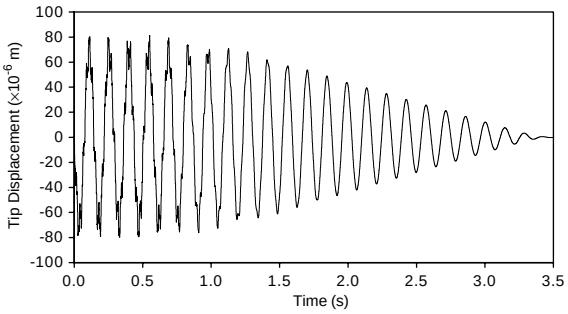

Fig. 10. Tip displacement of piezolaminated cantilever beam subjected to 0.2 N impact load at the tip and controlled using Lyapunov feedback (feedback: 0.1 V).

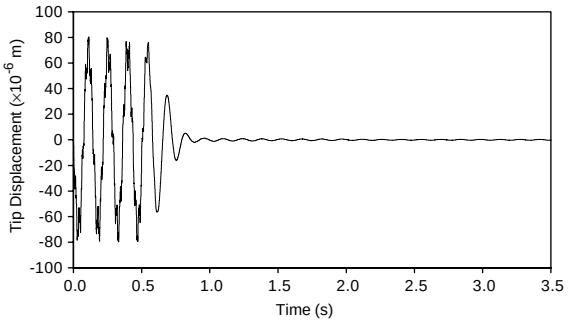

Fig. 11. Tip displacement of piezolaminated cantilever beam subjected to 0.2 N impact load at the tip and controlled using Lyapunov feedback (feedback: 1 V).

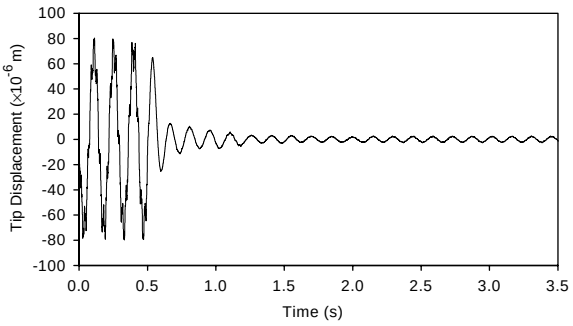

Fig. 12. Tip displacement of piezolaminated cantilever beam subjected to 0.2 N impact load at the tip and controlled using Lyapunov feedback (feedback voltage 9 V).

constant-gain negative velocity feedback and LQR control are shown in Table 2. It can be noted that LQR optimal control offers an effective control with lesser peak actuator voltages. In the present case, the gain of the constant-gain negative velocity feedback should be less than 3, due to the limitation of the maximum allowable voltage of the PZT used (that is, 2V/μm).

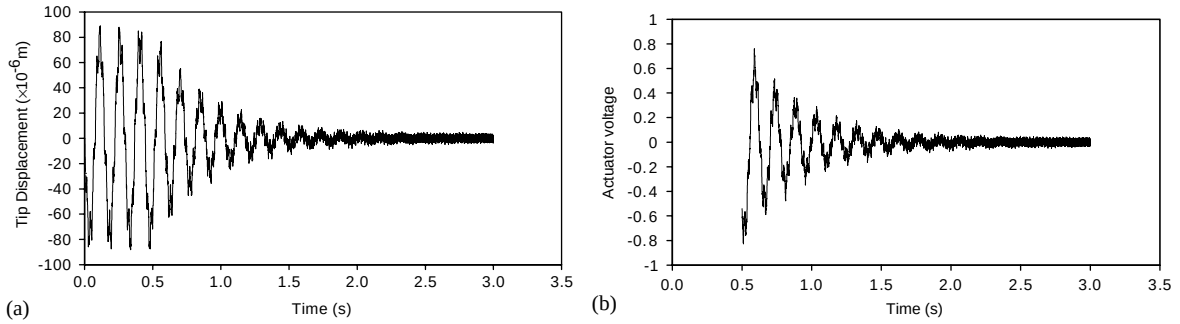

Fig. 13. (a) Tip displacement of piezolaminated cantilever beam subjected to 0.2 N impact load at the tip and controlled using LQR control ($Q=10^8$, $R=1$). (b) The actuator voltage.

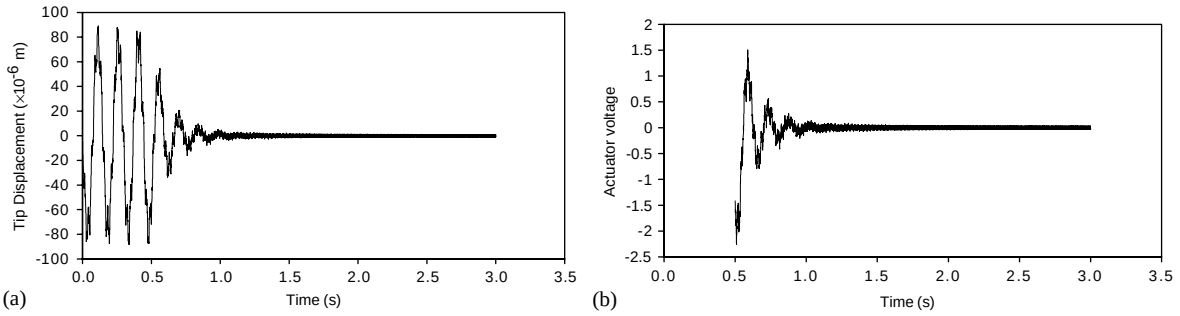

Fig. 14. (a) Tip displacement of piezolaminated cantilever beam subjected to 0.2 N impact load at the tip and controlled using LQR control ($Q=10^9$, $R=1$). (b) The actuator voltage.

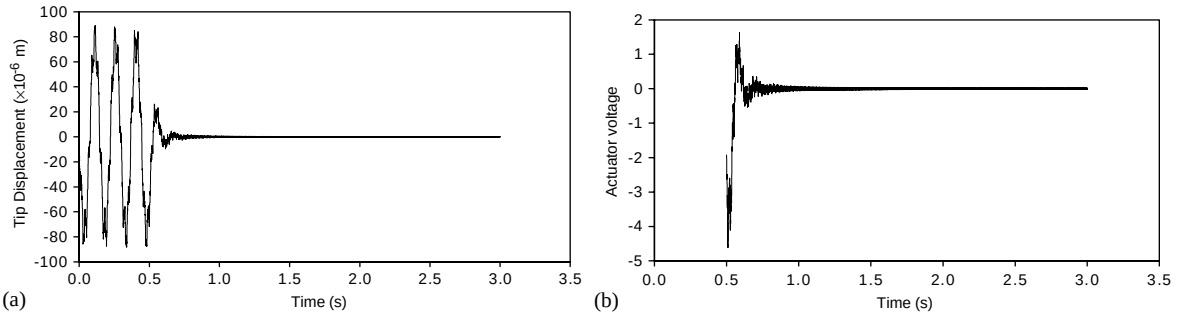

Fig. 15. (a) Tip displacement of piezolaminated cantilever beam subjected to 0.2 N impact load at the tip and controlled using LQR control ($Q=10^{10}$, $R=1$). (b) The actuator voltage.

The effectiveness of the active control strategy in controlling the response of the beam subjected to harmonic load are demonstrated in Figs. 16 and 17 wherein harmonic loads of $0.2\sin(250t)$ and $0.2\sin(43.3t)$ N are applied respectively at the free end. It can be noted that in the case indicated by Fig. 17, the harmonic load applied is near the first natural frequency.

Table 2
Damping ratio and peak actuator voltages for constant-gain negative velocity feedback and LQR control with different values of control parameters

Type of control strategy	First mode damping ratios	Peak actuator voltages
Constant-gain negative velocity feedback control (gain = 1)	0.0781	28.688
Constant-gain negative velocity feedback control (gain = 2)	0.1560	57.376
Constant-gain negative velocity feedback control (gain = 3)	0.2330	86.064
LQR control ($Q = 10^8$, $R = 1$)	0.0589	0.9480
LQR control ($Q = 10^8$, $R = 2$)	0.0421	0.6696
LQR control ($Q = 10^9$, $R = 1$)	0.1742	3.0000
LQR control ($Q = 10^{10}$, $R = 1$)	0.3815	8.9800

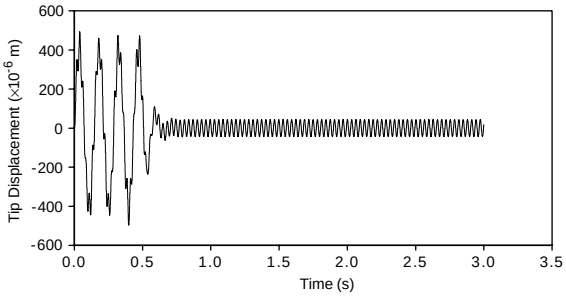

Fig. 16. Tip displacement of piezolaminated cantilever beam subjected to harmonic load of $0.2\sin(250t)$ N at the tip and controlled using constant-gain negative velocity feedback (gain = 1).

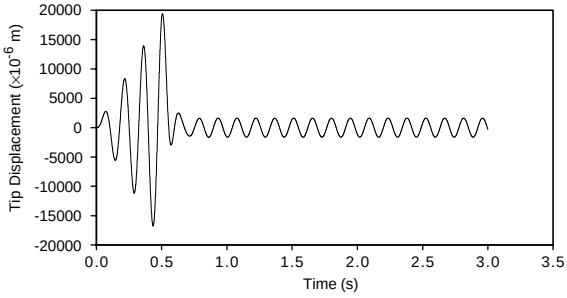

Fig. 17. Tip displacement of piezolaminated cantilever beam subjected to harmonic load of $0.2\sin(43.3t)$ N at the tip and controlled using constant-gain negative velocity feedback (gain = 1).

5.2. *Vibration control using piezolaminated plate/shell elements*

The piezolaminated plate/shell element has been validated for the sensing and actuation performance of the piezoelectric sensors and actuators without considering the thermal effects [26]. To demonstrate the correctness of the present formulation in solving the problems of thermal

Table 3
Non-dimensional central deflection of isotropic plate subjected to linear temperature distribution varying through the thickness for simply supported boundary condition

	Khdeir and Reddy [30]	Present model
Non-dimensional central deflection (W/h)	0.19079×10^{-4}	0.19139×10^{-4}

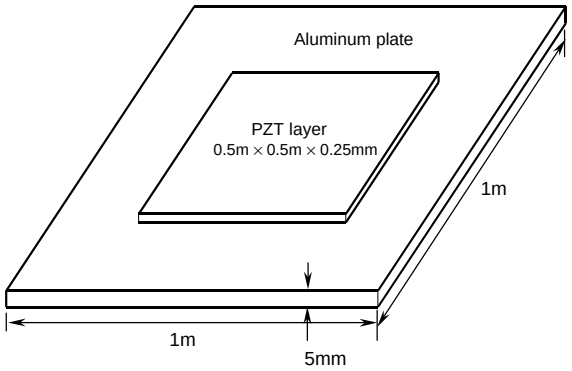

Fig. 18. Piezolaminated aluminum plate.

stress, a case for which closed form/exact solutions are available has been solved using the present formulation and results are compared with exact solutions. The temperature distribution, without any external load, is assumed as $T(x, y, z) = 2z$. In Table 3, non-dimensional displacement $\bar{w} = w/h$ at the center of the plate (length to breadth ratio $a/b = 1$, length to thickness ratio, $a/h = 100$ with simply supported boundary conditions is compared with those of the closed form/exact solution [30]. Other parameters considered in the above case are $v = 0.3, \alpha = 1 \times 10^{-6}, E = 1 \times 10^{7}$. It can be observed that the results based on the present formulation agree well with the available solutions.

5.2.1. Piezothermoelastic behavior and control of a simply supported piezolaminated plate

Piezothermoelastic behavior and control of a simply supported piezolaminated aluminum plate has been studied. The piezolaminated model considered (Fig. 18) is an aluminum plate 1 m × 1 m × 0.005 m sandwiched between two PZT layers of 0.5 m × 0.5 m size and 250 μm thickness. This plate has been modelled using the present piezolaminated plate element. The mesh size of 8×8 has been used. Material properties are summarized in Table 4. It is assumed that all the material properties are constant over the temperature range studied in this work. Three cases were considered. In the first case, the piezothermoelastic effect (sensing capability) of the distributed piezoelectric sensor due to thermal excitation has been considered. The second case is to examine the deflection due to the thermal gradient. The third case is to demonstrate a control method to simultaneously control the dynamic deflection and thermally induced static deflection.

Piezothermoelastic effect: voltage generation in the PZT sensor due to elevated temperature field. It has been assumed that the plate with the PZT sensor and actuator is placed in an elevated temperature field and the plate temperature quickly reaches a steady state. From Eq. (38), it can

Table 4
Material properties used

Properties	PZT piezoceramic	Aluminum
Young's modulus, E (N/m^2)	63.0×10^9	6.8×10^{10}
Density, ρ (kg/m^3)	7600.0	2800.0
Poisson's ratio, v	0.3	0.32
Coefficient of thermal expansion, α ($^\circ$C^{-1})	1.2×10^{-4}	23.8×10^{-6}
Piezoelectric strain constant, d_{31} and d_{32} (m/V)	1.79×10^{-10}	—
Electric permittivity, $\epsilon_{11} = \epsilon_{22} = \epsilon_{33}$ (F/m)	1.65×10^{-8}	—
Pyroelectric constant, P_3 (C/m^2/K)	0.25×10^{-4}	—

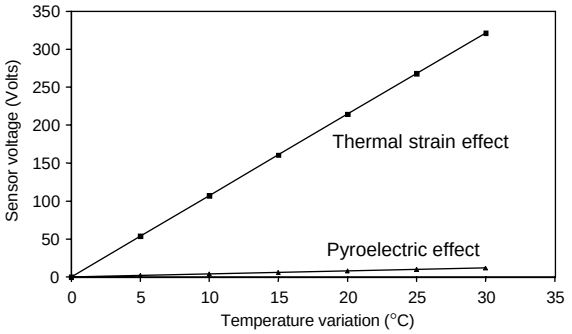

Fig. 19. Sensor voltage generated due to thermal excitation (–■–, thermal strain effect; –▲–, pyroelectric effect).

be noted that the temperature variation can induce an output voltage in the PZT sensor—*the pyroelectric effect*. In addition, the thermally induced deformation can also induce a sensor signal. This piezothermoelastic effect has been studied and these two sensor voltages are as shown in Fig. 19. It can be noted that the thermal strain effect is more significant than the pyroelectric effect on the piezoelectric layers.

Thermally induced deflection. In this case, a temperature gradient has been applied to the piezolaminated plate such that the temperature of the bottom surface is higher than the top surface. Due to this temperature gradient the middle of the plate deflects upwards. Fig. 20 indicates the centerline deflection of the plate for 5°C, 10°C, 20°C and 50°C temperature gradients.

Active vibration control with prescribed thermal gradient. An initial velocity of 1 m/s has been imposed on the middle of the plate and active vibration control performance has been studied using a LQR control scheme with weighting parameters $Q = 10^8$ and $R = 1$. The controller is switched on after 2 s and a natural structural damping of 1% has been assumed. Figs. 21 and 22 show the controlled center displacement versus time and actuator voltage versus time for the case where there is no thermal gradient. Figs. 23 and 24 indicate the controlled center displacement and actuator voltage for the piezolaminated plate subjected to a thermal gradient of 5°C when

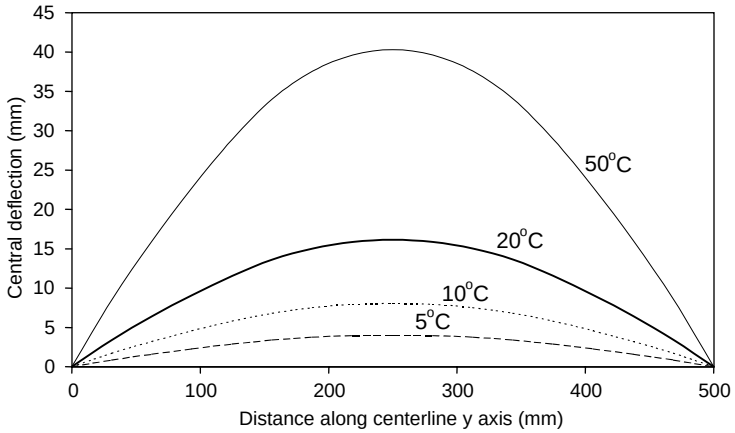

Fig. 20. Deflection due to thermal gradients (——, 50°C; ——, 20°C; ....., 10°C; – – – –20°C).

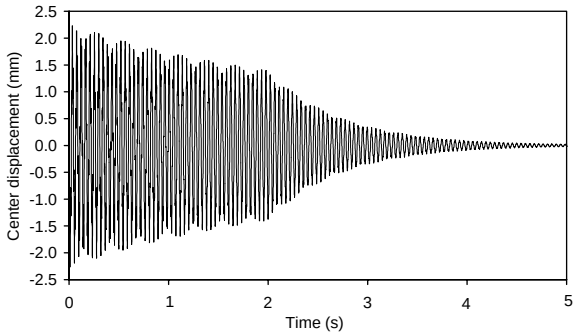

Fig. 21. Controlled dynamic response without thermal effect ($Q = 10^8$, $R = 1$).

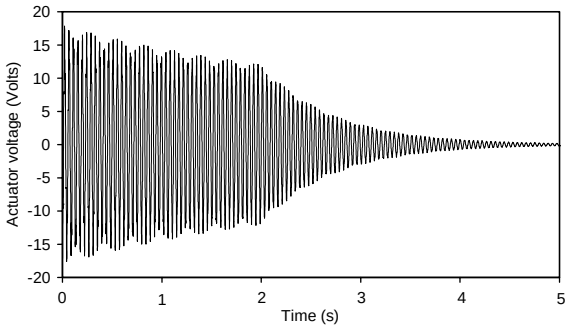

Fig. 22. Actuator voltage corresponding to Fig. 21.

subjected to a initial tip velocity of 1 m/s. It can be noted from Fig. 23 that there is thermally induced offset, due to a temperature gradient of 5°C in the controlled response. That is, the thermally induced offset is not controlled using the LQR scheme, which are only effective for the control of dynamic oscillation. With the result that a static offset is still there even after the

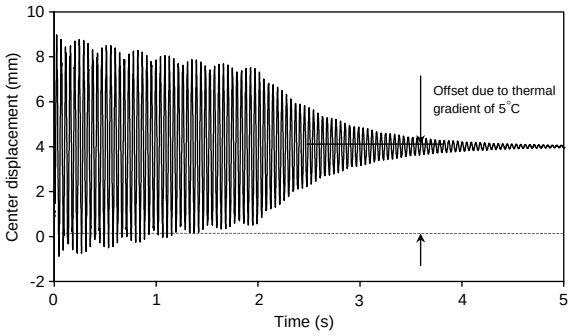

Fig. 23. Controlled dynamic response and actuator voltage with a thermal gradient of 5°C ($Q=10^8$, $R=1$).

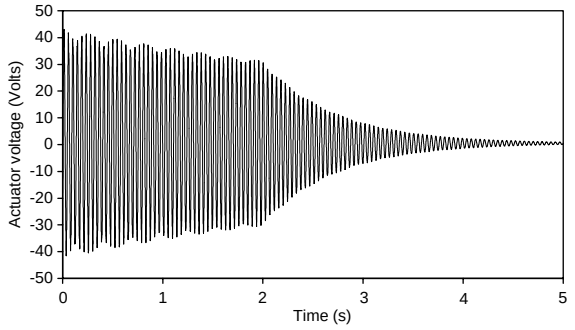

Fig. 24. Actuator voltage corresponding to Fig. 23.

dynamic oscillations have been controlled. If the original equilibrium position is desired then we have to control simultaneously both the thermally induced static deflection as well as the dynamic oscillation, which need two control voltages, one to control the dynamic oscillation and the other to control the thermally induced static deflection.

Active control of both the static deflection due to thermal gradient and dynamic deflection simultaneously. Fig. 25 shows the reduction in the thermally induced static offset due to a static voltage of 600 V applied to both the piezoelectric layers (sensor and actuator layers) apart from the dynamic control voltage. Fig. 26 shows how the static deflection is gradually reduced with the increase of the static voltage applied to the sensor and actuator. Thus, in order to completely control the plate, two control voltages need to be applied to the distributed piezoelectric layers, one to compensate the thermally induced deflection and the other to control the dynamic oscillations. It can be noted that the static control voltages needed to compensate the thermally induced static deflection is quite high even for a small thermal gradient of 5°C. It should be noted that excessively high actuator voltages have to be avoided so as to avoid depoling of the PZT. Generally, the allowed field strength for a particular class/type of piezoelectric material is specified by the manufacturer. Generally, it is $2\,V/\mu m$ and for the present case of 0.25 mm actuator thickness the breakdown voltage is 500 V. And hence, the PZT could not be effectively used to compensate the static deflection induced due to the thermal gradient as it needs very high DC voltage to be applied even for a small thermal gradient. Also it can be noted that the thermal

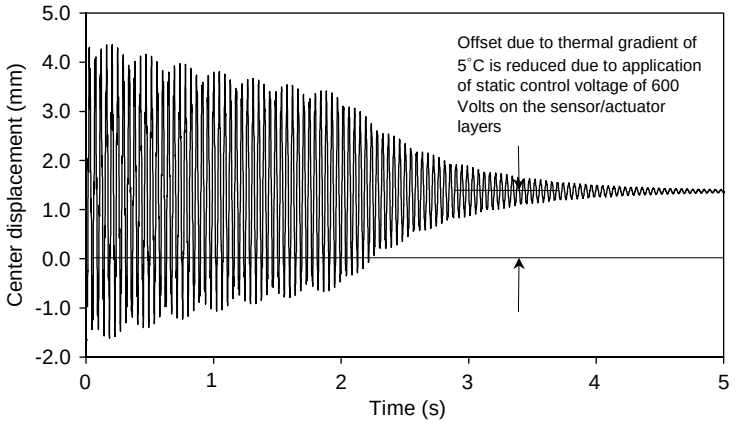

Fig. 25. Controlled dynamic response along with the static control voltage to control the offset due to the thermal gradient of 5°C (offset due to thermal gradient of 5°C is reduced due to application of static control voltage of 600 V on the sensor/actuator layers).

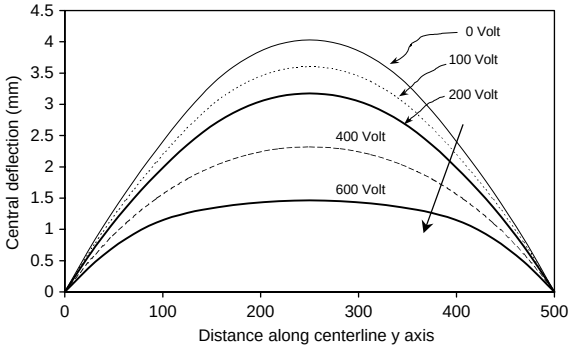

Fig. 26. Static control of the thermally induced static deflection (——, 0 V; ....., 100 V; ——, 200 V; – – – –, 400 V; ——, 600 V).

gradient is a constant loading and hence is not tracked/controlled automatically by the LQR control. This in a way is advantageous; otherwise excessive actuator voltages would be developed when these piezolaminated smart structures are kept in a high-temperature environment, damaging the PZT actuator. However, the transient displacement due to the sudden application/removal of the thermal gradient can be controlled by LQR. This is shown by Figs. 27 and 28. In this case, the controller is switched on after 2 s of the application of the initial velocity. The thermal gradient is applied at 2.5 s and removed at 4.0 s. The figures indicate that the transient displacement due to the application/removal of the thermal gradients is effectively controlled by LQR while the static offset exists when the thermal gradient exists.

5.2.2. Active vibration control of a cantilevered composite plate using classical controllers

A cantilevered laminated composite plate of dimension $0.5\,\text{m} \times 0.05\,\text{m} \times 0.01\,\text{m}$ with both the upper and lower surfaces symmetrically bonded with piezoceramic is considered. The plate

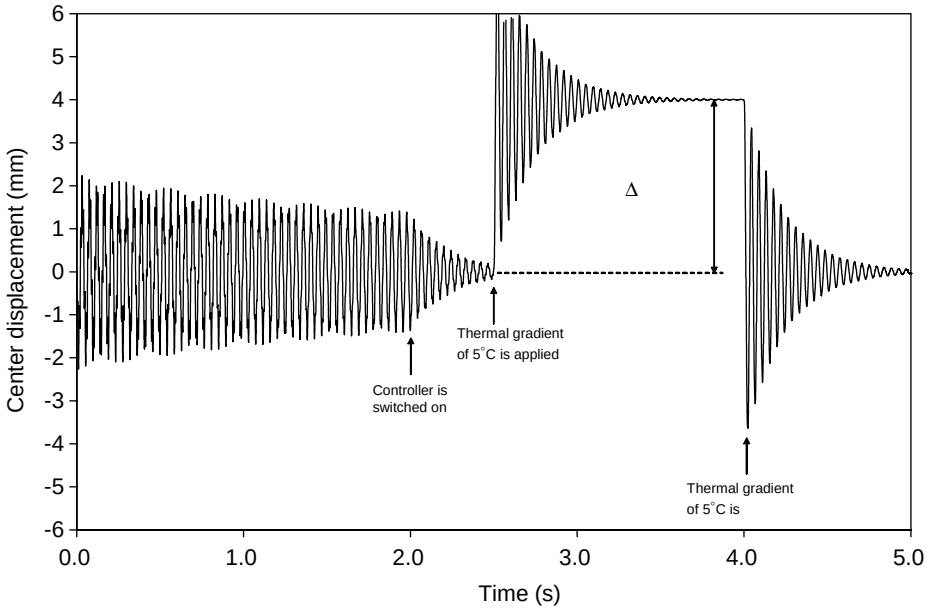

Fig. 27. Controlled dynamic response when the thermal gradient of 5°C is applied, maintained for 1.5 s and removed ($Q = 10^9$, $R = 1$).

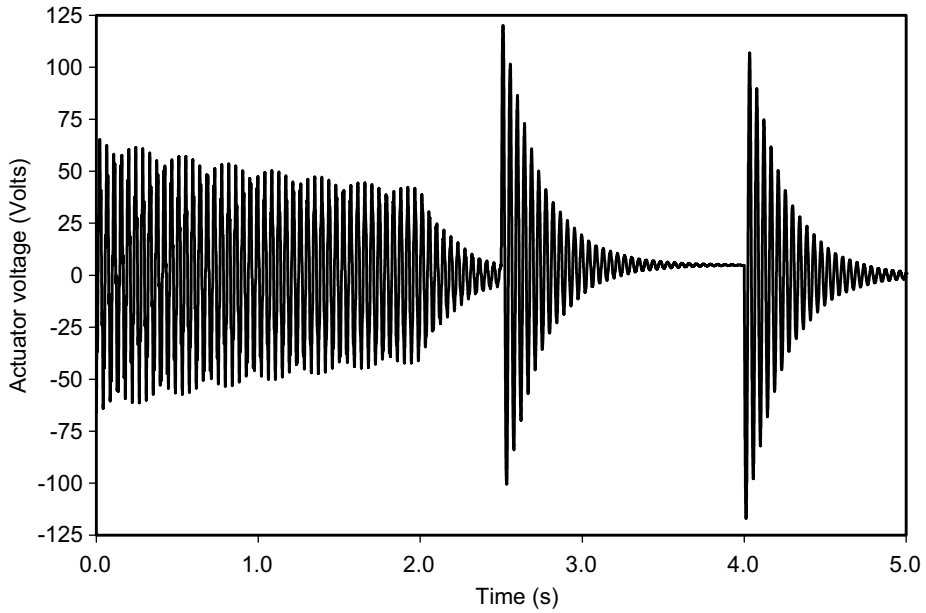

Fig. 28. Actuator voltage when the thermal gradient of 5°C is applied, maintained for 1.5 s and removed ($Q = 10^9$, $R = 1$) corresponding to Fig. 27.

Table 5
Material properties used

Properties	PZT piezoceramic	T300/976
Young's modulus, E_{11}, N/m^2	63.0×10^9	150×10^9
Young's modulus, $E_{22} = E_{33}$, N/m^2	63.0×10^9	9.0×10^9
Poisson's ratio, $v_{12} = v_{13} = v_{23}$	0.3	0.3
Shear modulus, G_{12}, N/m^2	24.2×10^9	7.1×10^9
Shear modulus, $G_{13} = G_{23}$ (N/m^2)	24.2×10^9	2.5×10^9
Density, ρ (kg/m^3)	7600.0	1600.0
Piezoelectric constant, d_{31} and d_{32} (m/V)	2.54×10^{-10}	—
Electric permittivity, $\epsilon_{11} = \epsilon_{22} = \epsilon_{33}$ (F/m)	1.53×10^{-8}	—

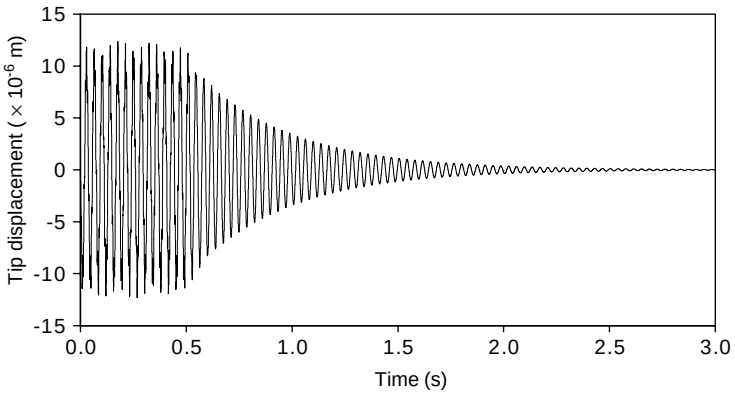

Fig. 29. Tip displacement of the piezolaminated composite plate controlled using constant-gain negative velocity feedback (gain = 1).

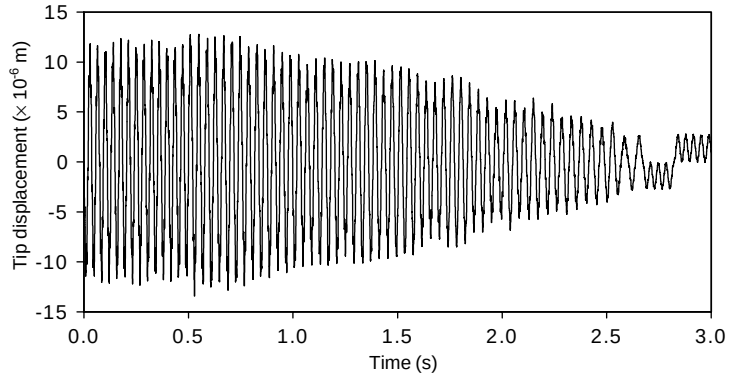

Fig. 30. Tip displacement of the piezolaminated composite plate controlled using Lyapunov feedback (1 V).

consists of four composite layers (−45/45/−45/45) of 2.5 mm thickness each. The piezoelectric layers are of thickness 0.1 mm each. The material properties are as shown in Table 5. An impulse load of 0.2 N for 1 ms is applied at the free end of the plate. As in the case of the beam the classical

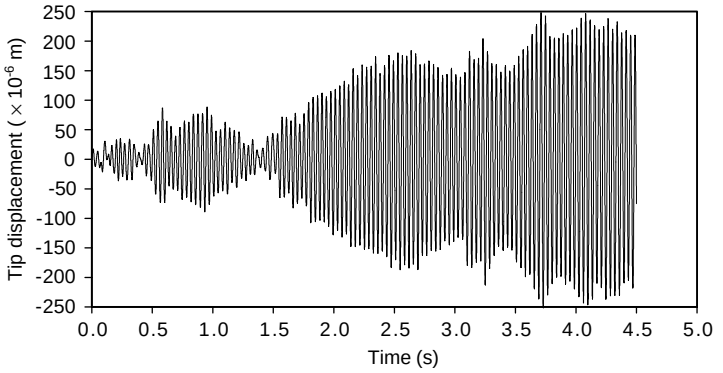

Fig. 31. Uncontrolled tip response of the piezolaminated composite plate due to the random loading at the tip (mean square response (MSR) = 1.03956×10^{-8}).

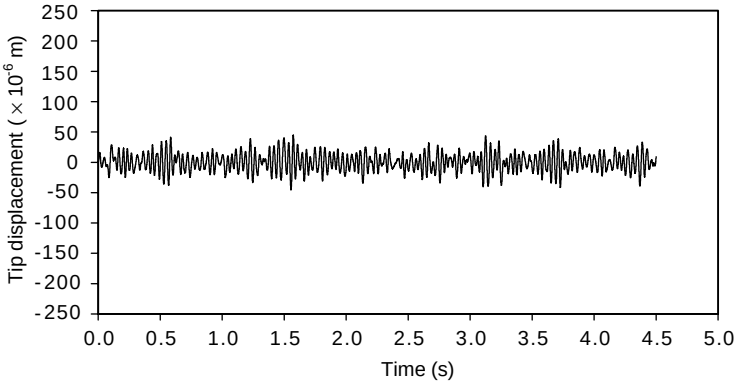

Fig. 32. Controlled tip response of the piezolaminated composite plate due to the random loading controlled using constant-gain negative velocity feedback (gain = 5) (mean square response (MSR) = 2.25384×10^{-10}).

control laws have been applied for active vibration control of piezolaminated plates. The dynamic response for constant-gain negative velocity feedback is shown in Fig. 29. Fig. 30 indicates the active control performance due to Lyapunov feedback. Then, the active control performance when the plate is subjected to random loading, which is a band-limited white noise of power spectral density $1 \times 10^{-6}\,\mathrm{N}^2/(\mathrm{rad/s})$ in the frequency range of 0–1000 rad/s, is considered. The uncontrolled and controlled responses at the free end of the plate are shown in Figs. 31 and 32 respectively. It can be noted that there is a reduction in mean square response (MSR) in the controlled case.

5.2.3. *Active vibration control of piezolaminated semicircular cantilevered steel shell*

A semicircular steel shell embedded with a PZT piezoceramic layers on the top and a bottom surface is considered as shown in Fig. 33. One end of the shell is fixed and the other end is free. It is 250 mm wide and 5 mm thick with an inner radius of 250 mm. The thicknesses of the PZT layers are 0.25 mm. The material properties of the PZT layers are $E_a = E_s = 63 \times 10^9\,\mathrm{N/m^2}$,

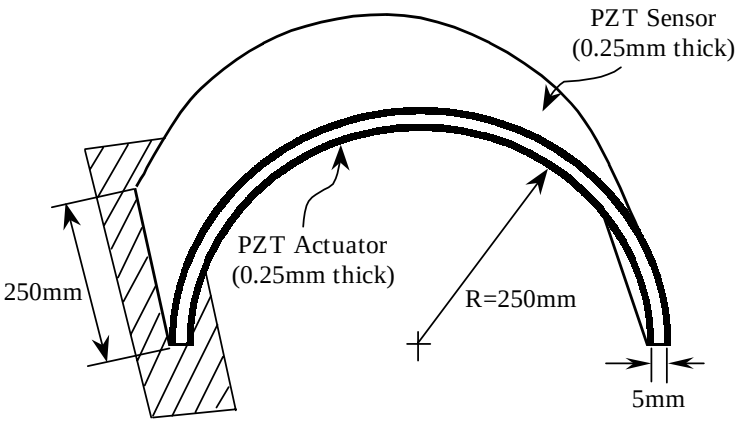

Fig. 33. Semicircular piezolaminated steel shell ($R = 250$ mm) with one end fixed (thickness of the steel shell 5 mm, thickness of PZT sensor 0.25 mm, thickness of PZT actuator 0.25 mm).

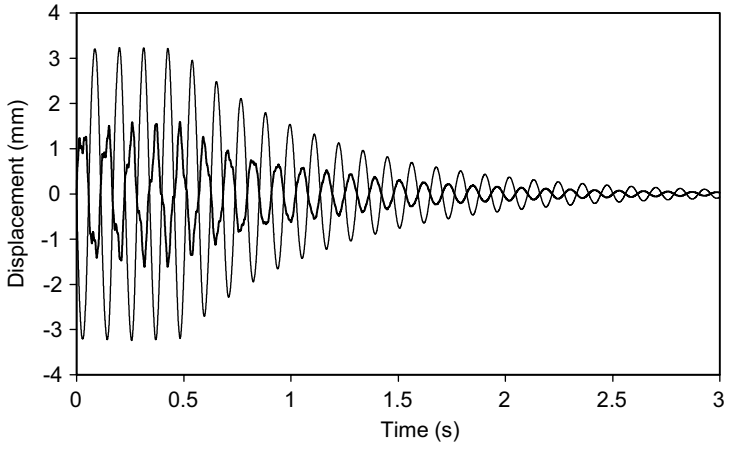

Fig. 34. Controlled tip response of the piezolaminated shell with 20% actuator coverage (along the hoop direction from the fixed end) (——, hoop displacement; ——, radial displacement).

$\rho_a = \rho_s = 7600\,\mathrm{kg/m^3}$, $v_a = v_s = 0.3$, $d_{31} = d_{32} = -1.79 \times 10^{-10}\,\mathrm{m/V}$, $\epsilon_{11} = \epsilon_{22} = \epsilon_{33} = 1.650 \times 10^{-8}\,\mathrm{F/m}$. The first six natural frequencies are 8.61, 14.85, 27.22, 63.19, 93.16 and 207.88 Hz (for a fully covered sensor and actuator layers). Among this the frequencies 14.85 and 63.19 Hz correspond to the modes in the width direction and hence do not participate in the radial and hoop direction response. An initial velocity of 0.5 m/s is applied to the free end of the shell along the hoop direction and the distributed vibration control of the shell with different lengths of actuators is investigated. Initial structural damping is assumed to be 0.2%. The SISO LQR scheme is used (with $Q = 10^{10}$ and $R = 1$). Figs. 34 and 35 show the tip responses and actuator voltages for 20% and 40% coverage of the actuators. Modal coupling between the first two transverse modes and hence control spillover are indicated clearly in Fig. 35. Fig. 36 indicates the frequency response plot comparing the uncontrolled and controlled responses. Fig. 37 summarizes the damping ratios for the first two transverse modes. It shows that the controlled

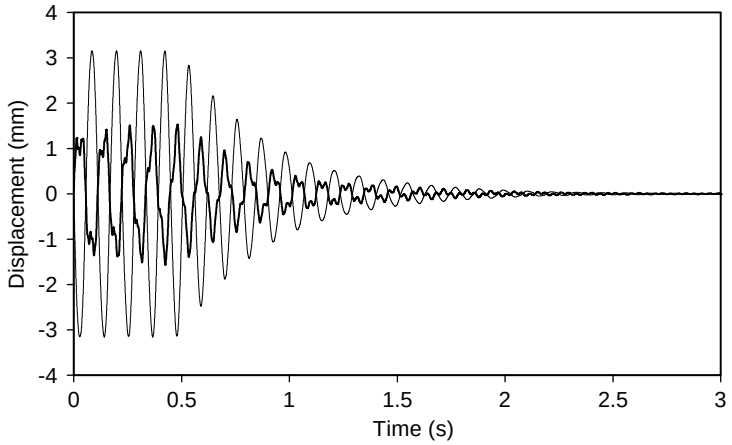

Fig. 35. Controlled tip response of the piezolaminated shell with 40% actuator coverage (along the hoop direction from the fixed end) (——, hoop displacement; ——, radial displacement).

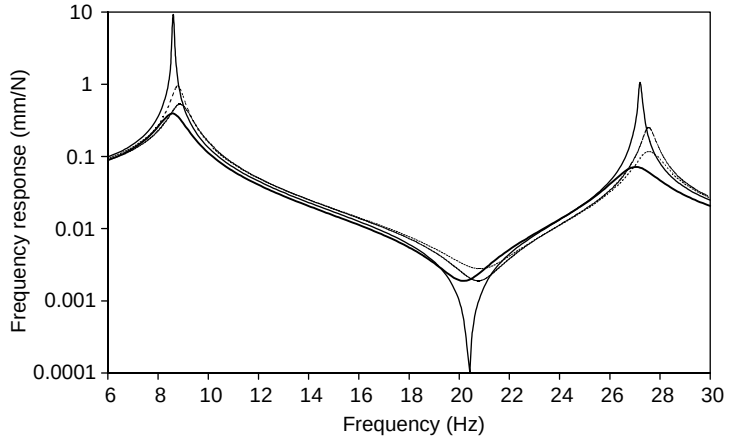

Fig. 36. Tip frequency response of the piezolaminated shell with and without control (——, no S/A coverage; ....., 20% S/A coverage; – – – –, 40% S/A coverage; ——, 100% S/A coverage).

damping ratio increases rather quickly as the extent of actuator coverage increases (from fixed end) upto 40% coverage and afterwards levels off at 70% coverage. It can also be observed that the second mode damping ratio initially increases upto 20% coverage and then decreases upto 40% coverage. This is due to the control spillover to the second mode. But as the extent of actuator coverage increases, the second mode damping ratio also increases and levels off at 80% coverage. It can be observed that we can get optimal vibration control performance with optimal cost using 60% actuator coverage.

Then the active vibration control of the above piezolaminated shell with 100% sensor/actuator coverage is studied with a specified thermal gradient. The inner surface of the shell is subjected to 25°C and the outer surface to 30°C with a thermal gradient of 5°C between inner and outer surface, and an initial velocity of 0.5 m/s is applied to the free end of the shell. The controlled

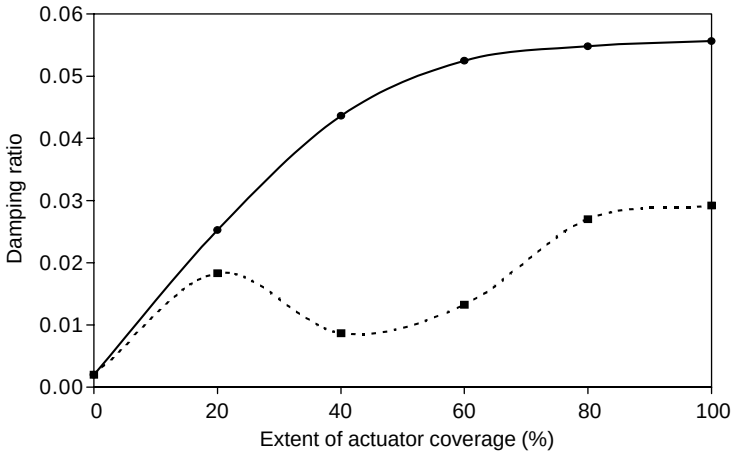

Fig. 37. Damping ratio versus extent of actuator coverage of the piezolaminated shell (along the hoop direction from the fixed end) (——, first mode; – – – –, second mode).

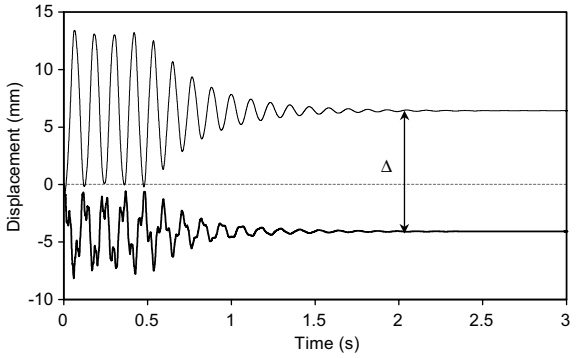

Fig. 38. Controlled tip response of the piezolaminated shell with 100% sensor/actuator coverage and thermal gradient of 5°C (——, hoop displacement; ——, radial displacement; Δ, offset due to thermal gradient of 5°C).

dynamic response for this case with LQR control ($Q = 10^{10}$ and $R = 1$) is as shown in Fig. 38. It can be noted that there is an offset due to the thermal gradient which is not controlled using LQR control. It can also be noted that there is a positive offset in the hoop displacement and negative offset in the radial displacement. As mentioned earlier this thermally induced offset can be compensated only by the application of a large DC control voltage to the sensor/actuator layers. Fig. 39 shows the controlled tip response with the LQR control and 500 V DC control voltage applied to the sensor/actuator layers. It can be noted that even with this high DC voltage, a complete reduction/compensation of the thermally induced static offset could not be achieved. Fig. 40 indicates the reduction in the thermally induced static displacement with the static control voltage. As mentioned in Section 5.2.1, the thermally induced static offset cannot be effectively controlled using piezoelectric actuators. However, the transient displacements due to sudden application of thermal gradients can be controlled effectively with piezoelectric actuators using a LQR controller.

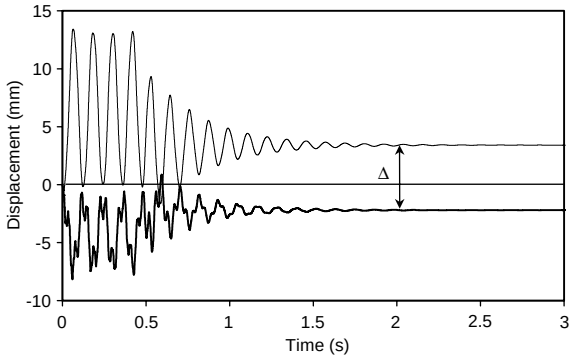

Fig. 39. Controlled tip response of the piezolaminated shell with 100% sensor/actuator coverage and thermal gradient of 5°C and static control voltage of 500 V applied to sensor/actuator (——, hoop displacement; ——, radial displacement; Δ, offset due to thermal gradient of 5°C is reduced due to the application of static control voltage).

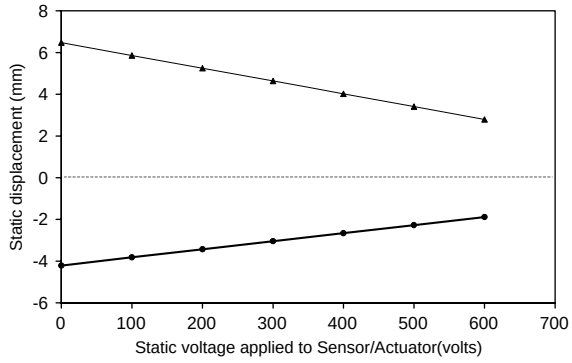

Fig. 40. Reduction in the thermally induced static displacement with the static control voltage applied to sensor/actuator (——, hoop displacement; ——, radial displacement).

6. Conclusions

In the present paper, shear deformable piezolaminated beam, plate and shell finite elements are formulated including the stiffness, mass and electromechanical coupling effects of distributed piezoelectric sensor and actuator layers. In the case of plate/shell elements the thermoelectromechanical coupling is also considered. The active vibration control performance of these piezolaminated structures are studied using classical control methods like constant-gain negative velocity feedback and Lyapunov feedback which are based on output feedback, and a modern control method, the linear quadratic regulator (LQR) scheme, which is an optimal control theory based on full state feedback. Their relative performance is discussed.

The study revealed that the LQR control scheme is very effective in controlling the vibration as the optimal gain is obtained minimizing the cost function. Classical control methods like constant-gain negative velocity feedback are quite simple and less effective.

A piezolaminated steel beam has been considered for the case studies. Thermally induced voltage generation in the distributed PZT sensors has been investigated. It has been shown that the sensor voltage contributed by the thermal strain effect is much more than that contributed by pyroelectric effect. The thermally induced static deflection due to the thermal gradients between top and bottom surfaces of the plate/shell has been investigated. Then the active control of the piezolaminated plate/shell subjected to thermal gradients has been studied. It has been shown that the thermal gradients induce a static deflection and if this needs to be compensated, we need to apply additional static control voltages and the magnitude of static control voltages needed are quite high even for a smaller thermal gradient. The deflection induced due to thermal gradient, being a static load cannot be controlled by the LQR control methods, which are effective only for dynamic control. However, the additional transient deflections due to the sudden application of the thermal gradients can be controlled by the LQR control method.

Appendix A. Nomenclature

$[A]$, $[A_{cl}]$	open- and closed-loop system matrices
A_b, A_p	cross-sectional area of beam and piezoelectric layer
A_a, A_s	cross-sectional area of piezoelectric sensor layer and piezoelectric actuator
$[B]$	control matrix
$[\hat{B}]$	disturbance matrix
$[B^{th}]$	thermal disturbance matrix
b	width of the beam
$[C]$	global damping matrix
$[\bar{C}]$	global damping matrix in modal co-ordinates
$[C_o]$	output matrix
D	electrical displacement
d_{31}, d_{32}	piezoelectric strain constants
$[d]$	piezoelectric strain constant matrix
$[e]$	piezoelectric stress constant matrix
$\{E\}$	electric field
E_b, E_a	young's modulus of beam material and piezoelectric material
E_a, E_s	young's modulus of piezoelectric actuator and piezoelectric sensor
P_c	control force vector
$\{\bar{P}_c\}$	control force vector in modal co-ordinates
$\{f_d\}$	disturbance force vector
$\{\bar{f}_d\}$	disturbance force vector in modal co-ordinates
$\{F_{eth}\}$, $\{F_{pth}\}$	thermal force vectors due to thermal strain effect and pyroelectric effect
$[G_c]$	gain matrix
I_b, I_s, I_a	moment of inertia of beam, piezoelectric actuator and sensor layers
$[K]$	global stiffness matrix
$[\bar{K}]$	global stiffness matrix in modal co-ordinates
$[K]_e$	element stiffness matrix

$[K_{uu}]$ element stiffness matrix
$[K_{u\phi}]$ element elastic–electric coupling stiffness matrix
$[K_{u\theta}]$ element thermomechanical coupling stiffness matrix
$[K_{\phi\theta}]$ element electrothermal stiffness matrix
$[K_{\phi\phi}]$ element electric stiffness matrix
k_α shear correction factor ($=5/6$)
L beam length
L_e element length
$[M]$ global mass matrix
$[M]_e$, $[M_{uu}]$ element mass matrices
$[\bar{M}]$ global mass matrix in modal co-ordinates
$\{F\}$, $\{M\}$, $\{S\}$ membrane, bending and shear force resultants
S_{p11} elastic compliance constant of piezoelectric materials
Q_{p11} elastic stiffness constant of piezoelectric materials
$[\tilde{P}]$ solution of the Riccati equation
$[Q]$, $[R]$ weighting matrices in the LQR scheme
R_x, R_y, R_z radii of curvatures in x, y and z directions
t time
h_a, h_s thickness of piezoelectric actuator and piezoelectric sensor
$\{u_d\}$ disturbance input vector
u, v, w displacement in x, y and z directions
$[N_w]$, $[N_\theta]$, $[N_u]$ shape function matrices for transverse displacement, rotation, axial displacement of the beam
y output vector
z co-ordinate in the transverse direction

Greek letters

λ, P stress coefficient of thermal expansion, pyroelectric coefficients
Θ global temperature variation in °C
$[\delta]$ global displacement vector
$\{\varepsilon\}$ dielectric constant matrix of piezoelectric material
$\{\epsilon_p\}$, $\{\epsilon_b\}$, $\{\epsilon_s\}$ inplane, bending and shear strains
ρ_b mass density of beam material
ρ_a, ρ_s mass density of piezoelectric actuator material and piezoelectric sensor material
θ rotation of the beam
θ_x, θ_y rotations in x and y directions in the shell
ω_j natural frequency of the jth mode
ϕ_a, ϕ_s, actuator and sensor voltage
$\{\phi_a\}$ control input vector
$\{\xi\}$ state vector

Subscripts

b, s, a beam, sensor and actuator
e elemental quantities

References

[1] T. Bailey, J.E. Hubbard, Distributed piezoelectric-polymer active vibration control of a cantilever beam, Journal of Guidance Control 8 (5) (1985) 605–611.

[2] E.F. Crawley, J.de. Luis, Use of piezoelectric actuators as elements of intelligent structures, American Institute of Aeronautics and Astronautics Journal 25 (10) (1987) 1373–1385.

[3] H.S. Tzou, Integrated distributed sensing and active vibration suppression of flexible manipulators using distributed piezoelectrics, Journal of Robotic Systems 6 (6) (1989) 745–767.

[4] H.S. Tzou, Piezoelectric Shells—Distributed Sensing and Control of Continua, Kluwer Academic, London, 1993.

[5] M.H.H. Shen, A new modeling technique for piezoelectrically actuated beams, Computers and Structures 57 (3) (1995) 361–366.

[6] C.K. Lee, Theory of laminated piezoelectric plates for the design of distributed sensors/actuators. Part I: governing equations and reciprocal relationships, Journal of Acoustical Society of America 87 (3) (1990) 1144–1158.

[7] H.S. Tzou, C.I. Tseng, Distributed modal identification and vibration control of continua: piezoelectric finite element formulation and analysis, American Society of Mechanical Engineers Journal of Dynamical Systems, Measurement Control 113 (1991) 500–505.

[8] S.K. Ha, C. Keilers, F.K. Chang, Finite element analysis of composite structures containing distributed piezoceramic sensors and actuators, American Institute of Aeronautics and Astronautics Journal 30 (3) (1992) 772–780.

[9] W.-S. Hwang, H.C. Park, Finite element modeling of piezoelectric sensors and actuators, American Institute of Aeronautics and Astronautics Journal 31 (5) (1993) 930–937.

[10] D.T. Detwiler, M.H.H. Shen, V.B. Venkayya, Finite element analysis of laminated composite structures containing distributed piezoelectric actuators and sensors, Finite Elements in Analysis and Design 20 (1995) 87–100.

[11] Z. Wang, S. Chen, W. Han, Static shape control for intelligent structures, Finite Elements in Analysis and Design 26 (1997) 303–314.

[12] K.Y. Lam, X.Q. Peng, G.R. Liu, J.N. Reddy, A finite element model for piezoelectric composite laminates, Smart Materials and Structures 6 (1997) 583–591.

[13] R. Lammering, The application of a finite shell element for composite containing piezoelectric polymers in vibration control, Computers and Structures 41 (5) (1991) 1101–1109.

[14] H.S. Tzou, M. Gadre, Theoretical analysis of a multi-layered thin shell coupled with piezoelectric shell actuators for distributed vibration controls, Journal of Sound and Vibration 132 (3) (1989) 433–450.

[15] H.S. Tzou, R. Ye, Analysis of piezoelectric structures with laminated piezoelectric triangular shell elements, American Institute of Aeronautics and Astronautics Journal 34 (1) (1996) 110–115.

[16] D.A. Saravanos, Mixed laminate theory and finite element for smart piezoelectric composite shell structures, American Institute of Aeronautics and Astronautics Journal 34 (8) (1997) 1327–1333.

[17] S.S. Rao, M. Sunar, Analysis of distributed thermopiezoelectric sensors and actuators in advanced intelligent structures, American Institute of Aeronautics and Astronautics Journal 31 (7) (1993) 1280–1286.

[18] H.S. Tzou, R. Ye, Piezothermoelasticity and precision control of piezoelectric systems: theory and finite element analysis, Journal of Vibration and Acoustics 116 (1994) 489–495.

[19] A.J. Lee, D.A. Saravanos, A coupled layerwise analysis of the thermopiezoelectric response of smart composite beams, NASA Technical Memorandum 106889 AIAA-95-1101, 1995.

[20] T.R. Tauchert, F. Ashida, N. Noda, S. Adali, V. Verijenko, Developments in thermopiezoelasticity with relevance to smart composite structures, Composite Structures 48 (2000) 31–38.

[21] IEEE Standard on Piezoelectricity, ANSI-IEEE Std 176-187, 1987.

[22] H. Kwakernaak, R. Sivan, Linear Optimal Control Systems, Wiley, New York, 1972.

[23] C.R. Fuller, S.J. Elliott, P.A. Nelson, Active Control of Vibration, Academic Press, London, 1996.

[24] B.P. Naganarayana, G. Prathap, B. Dattaguru, B.S. Ramamurthy, A field consistent and variationally correct representation of transverse shear strain in nine noded plate element, Computer Methods in Applied Mechanics and Engineering 97 (1992) 355–374.

[25] M. Ganapathi, T.K. Varadan, V. Balamurugan, Dynamic instability of anisotropic laminated composite curved panels using finite element method, Computers and Structures 53 (2) (1994) 335–342.

[26] V. Balamurugan, S. Narayanan, Shell finite elements for smart piezoelectric composite plates/shells structures and its application to the study of active vibration control, Finite Elements in Analysis and Design 37 (9) (2001) 713–738.
[27] R.M. Jones, Mechanics of Composite Materials, McGraw-Hill, New York, 1975.
[28] V. Balamurugan, S. Narayanan, Active vibration control of piezolaminated smart beams, Defence Science Journal 51 (2) (2001) 103–114.
[29] A. Baz, S. Poh, Performance of an active control system with piezoelectric actuators, Journal of Sound and Vibration 126 (2) (1988) 327–343.
[30] A.A. Khdeir, J.N. Reddy, Thermal stresses and deflections of cross-ply laminated plates using refined plate theories, Journal of Thermal Stresses 14 (4) (1991) 419–438.